ANTIOXIDANTS & REDOX SIGNALING
Volume 23, Number 18, 2015

DOI: 10.1089/ars.2014.6221

ORIGINAL RESEARCH COMMUNICATION

NOX4 NADPH Oxidase-Dependent Mitochondrial Oxidative Stress in Aging-Associated Cardiovascular Disease

Aleksandr E. Vendrov,[1] Kimberly C. Vendrov,[2] Alberto Smith,[3] Jinling Yuan,[1] Arihiro Sumida,[1] Jacques Robidoux,[4] Marschall S. Runge,[1,*] and Nageswara R. Madamanchi[1,*]

Abstract

Aims: Increased oxidative stress and vascular inflammation are implicated in increased cardiovascular disease (CVD) incidence with age. We and others demonstrated that NOX1/2 NADPH oxidase inhibition, by genetic deletion of *p47phox*, in $Apoe^{-/-}$ mice decreases vascular reactive oxygen species (ROS) generation and atherosclerosis in young age. The present study examined whether NOX1/2 NADPH oxidases are also pivotal to aging-associated CVD. ***Results:*** Both aged (16 months) $Apoe^{-/-}$ and $Apoe^{-/-}/p47phox^{-/-}$ mice had increased atherosclerotic lesion area, aortic stiffness, and systolic dysfunction compared with young (4 months) cohorts. Cellular and mitochondrial ROS (mtROS) levels were significantly higher in aortic wall and vascular smooth muscle cells (VSMCs) from aged wild-type and $p47phox^{-/-}$ mice. VSMCs from aged mice had increased mitochondrial protein oxidation and dysfunction and increased vascular cell adhesion molecule 1 expression, which was abrogated with (2-(2,2,6,6-Tetramethylpiperidin-1-oxyl-4-ylamino)-2-oxoethyl)triphenylphosphonium chloride (MitoTEMPO) treatment. NOX4 expression was increased in the vasculature and mitochondria of aged mice and its suppression with shRNA in VSMCs from aged mice decreased mtROS levels and improved function. Increased mtROS levels were associated with enhanced mitochondrial NOX4 expression in aortic VSMCs from aged subjects, and NOX4 expression levels in arterial wall correlated with age and atherosclerotic severity. Aged $Apoe^{-/-}$ mice treated with MitoTEMPO and 2-(2-chlorophenyl)-4-methyl-5-(pyridin-2-ylmethyl)-1H-pyrazolo[4,3-c]pyridine-3,6(2H,5H)-dione had decreased vascular ROS levels and atherosclerosis and preserved vascular and cardiac function. ***Innovation and Conclusion:*** These data suggest that NOX4, but not NOX1/2, and mitochondrial oxidative stress are mediators of CVD in aging under hyperlipidemic conditions. Regulating NOX4 activity/expression and using mitochondrial antioxidants are potential approaches to reducing aging-associated CVD. *Antioxid. Redox Signal.* 23, 1389–1409.

Introduction

OVER HALF OF Americans suffering from cardiovascular diseases (CVDs) are 60 years of age or older, and the prevalence of CVD doubles with advancing age (18). Indeed, age is an independent nonmodifiable risk factor for atherosclerosis and coronary artery disease (39). The pathophysiology of atherosclerotic plaque formation has been extensively studied and is characterized by endothelial dysfunction and/or arterial injury, followed by inflammatory cell migration into the vessel wall, oxidized lipid deposition, and cellular proliferation and increased fibrosis, with a resulting state of chronic

[1]Department of Medicine, McAllister Heart Institute, University of North Carolina, Chapel Hill, North Carolina.
[2]Division of Pharmacotherapy and Experimental Therapeutics, Eshelman School of Pharmacy, University of North Carolina, Chapel Hill, North Carolina.
[3]Cardiovascular Division, Academic Department of Surgery, National Institute for Health Research Biomedical Research Center at Guy's and St Thomas' National Health Service Foundation Trust, King's College London British Heart Foundation Centre of Excellence, London, United Kingdom.
[4]Department of Pharmacology and Toxicology, The East Carolina Diabetes and Obesity Institute, East Carolina University, Greenville, North Carolina.
*Both authors were joint senior authors.

Innovation

NOX1/NOX2 NADPH oxidase inhibition in *Apoe*$^{-/-}$ mouse, a model of human atherosclerosis, attenuated atherogenesis in young, but not in old, age. Instead, increased Nox4 expression/activity correlated with increased mitochondrial oxidative stress, mitochondrial and cardiovascular dysfunction, and atherosclerosis in aged *Apoe*$^{-/-}$ and *Apoe*$^{-/-}$*/p47phox*$^{-/-}$ mice. NOX4 expression is correlated with aging and increased in human atherosclerotic arteries. 2-(2-Chlorophenyl)-4-methyl-5-(pyridin-2-ylmethyl)-1H-pyrazolo[4,3-c]pyridine-3,6(2H,5H)-dione, an NOX1/NOX4 inhibitor, and (2-(2,2,6,6-tetramethylpiperidin-1-oxyl-4-ylamino)-2-oxoethyl)triphenylphosphonium chloride, a mitochondrial antioxidant, attenuated aging-associated increase in atherosclerosis and vascular dysfunction. Improvement of cardiac dysfunction in aging by the inhibition of NOX4 NADPH oxidase activity suggests that NOX4 is a potential therapeutic target for aging-associated cardiovascular disease.

inflammation (31, 33, 52). Reactive oxygen species (ROS)-mediated signaling pathways have been implicated as a common mechanism linking various atherosclerosis risk factors to plaque formation and clinical manifestations of atherosclerosis (28, 32).

Aging is associated with increased ROS levels in multiple tissues, including the vasculature. Vascular smooth muscle cells (VSMCs) from aged mice had increased ROS generation and significantly higher indices of cellular and mitochondrial oxidative damage in response to thrombin treatment (37). Mitochondrial DNA damage was also increased with age in mouse aortas (4). Aging-induced vascular dysfunction, including atherosclerosis, has been attributed to a proinflammatory shift in vascular gene expression, induction of apoptosis, and decreased mitochondrial biogenesis caused by increased mitochondrial oxidative stress (57). However, the precise molecular mechanisms that mediate the increase of atherosclerosis in aging have not been fully elucidated.

NADPH oxidases (NOXs) and mitochondria are the major source of ROS in vascular cells in both normal and pathological conditions. Depending on the cell type, NOX1, NOX2, and NOX4 homologs together with p22phox make up the membrane-bound catalytic core (8). We previously demonstrated that deletion of p47phox subunit and the resultant inactivation of NOX1/2-dependent NADPH oxidases in young atherosclerosis-susceptible *Apoe*$^{-/-}$ mice decreased vascular ROS levels, lowered adhesion molecule expression and macrophage infiltration into atherosclerotic lesions, and reduced atherosclerotic burden (5, 61). Supporting our data, Judkins *et al.* (25) reported that deletion of *Nox2* in *Apoe*$^{-/-}$ mice decreased ROS levels, increased NO bioavailability, and reduced aortic atherosclerosis. Sheehan *et al.* (48) demonstrated that *Apoe*$^{-/-}$*/Nox1*$^{-/y}$ mice had reduced aortic superoxide levels and atherosclerotic lesion area with decreased macrophage infiltration compared with *Apoe*$^{-/-}$ mice. Increased NOX expression and activity have also been correlated with the severity of atherosclerosis in humans (49).

NOX4-dependent NOX, in contrast to NOX1/2-dependent enzymes, does not require cytosolic regulatory subunits for activation and its activity is regulated at the expression level, generating predominantly H_2O_2 (41, 47, 54). NOX4 is ubiquitously expressed, including in VSMCs that constitute the bulk of the vascular wall. Recent reports suggest that NOX4 is localized to mitochondria, wherein it contributes to ROS levels (1, 6).

Most studies of mitochondrial ROS (mtROS) generation have focused on events that occur after oxidative damage to electron transport chain (ETC) complexes under pathophysiological conditions, including changes in ROS generation as a result of ETC uncoupling or decreased superoxide scavenging as a result of reduced expression of the superoxide dismutase 2 (SOD2). Increased mtROS results in mtDNA damage, oxidation of mitochondrial proteins, and further mitochondrial dysfunction (31). Mitochondrial-derived ROS also likely enter the cytoplasm and activate intracellular signaling pathways, leading to endothelial dysfunction and inflammation (23). However, the primary triggers that lead to ETC uncoupling with aging are not well understood.

This study was aimed at understanding the roles of NOXs in age-associated atherosclerosis and impairment of vascular and cardiac function, with the goal of formulating strategies to identify potential preventive and therapeutic interventions. Because wild-type mice do not exhibit significant cardiovascular changes with age (66), we performed cardiovascular phenotyping in hypercholesterolemic young and aged *Apoe*$^{-/-}$ and *Apoe*$^{-/-}$*/p47phox*$^{-/-}$ mice. We found that in contrast to the effect in young (4-month-old, 4 mo) mice, NOX1/2 NADPH oxidase inhibition failed to attenuate atherosclerosis in aged (16-month-old, 16 mo) *Apoe*$^{-/-}$*/p47phox*$^{-/-}$ mice. The lack of protection was correlated with increase in ROS levels and NOX4 expression in VSMCs and aortas of aged mice, as well as increased mtROS levels in VSMCs.

In addition, aged *Apoe*$^{-/-}$ and *Apoe*$^{-/-}$*/p47phox*$^{-/-}$ mice had impaired vascular and cardiac function. Increased NOX4 expression in VSMCs of aged mice was associated with increased mitochondrial dysfunction, and suppression of NOX4 in VSMCs attenuated mtROS levels and improved mitochondrial function. NOX4 expression also increased with age in both human aortic VSMCs and carotid arteries. Administration of mitochondria-targeted antioxidant (2-(2,2,6,6-tetramethylpiperidin-1-oxyl-4-ylamino)-2-oxoethyl)-triphenylphosphonium chloride (MitoTEMPO) and the selective NOX1/NOX4 inhibitor 2-(2-chlorophenyl)-4-methyl-5-(pyridin-2-ylmethyl)-1H-pyrazolo[4,3-c]pyridine-3,6(2H,5H)-dione (AK120765) to aged *Apoe*$^{-/-}$ mice decreased aortic oxidative stress and atherosclerosis and improved aortic compliance. Together, these data indicate that NOX4 NADPH oxidase plays an important role in age-associated increase in mtROS levels and mitochondrial dysfunction, vascular dysfunction, and atherosclerosis, particularly in hyperlipidemic conditions.

Results

NOX1/2 NADPH oxidase inhibition in aged Apoe$^{-/-}$ *mice does not result in decreased vascular ROS levels and atherosclerosis*

To examine the interplay of ROS, aging, and atherogenesis, we first determined atherosclerotic burden in young and aged *Apoe*$^{-/-}$ and *Apoe*$^{-/-}$*/p47phox*$^{-/-}$ mice fed normal chow or Western diet (Fig. 1). Consistent with our previous findings (5, 62), young *Apoe*$^{-/-}$*/p47phox*$^{-/-}$ on a Western

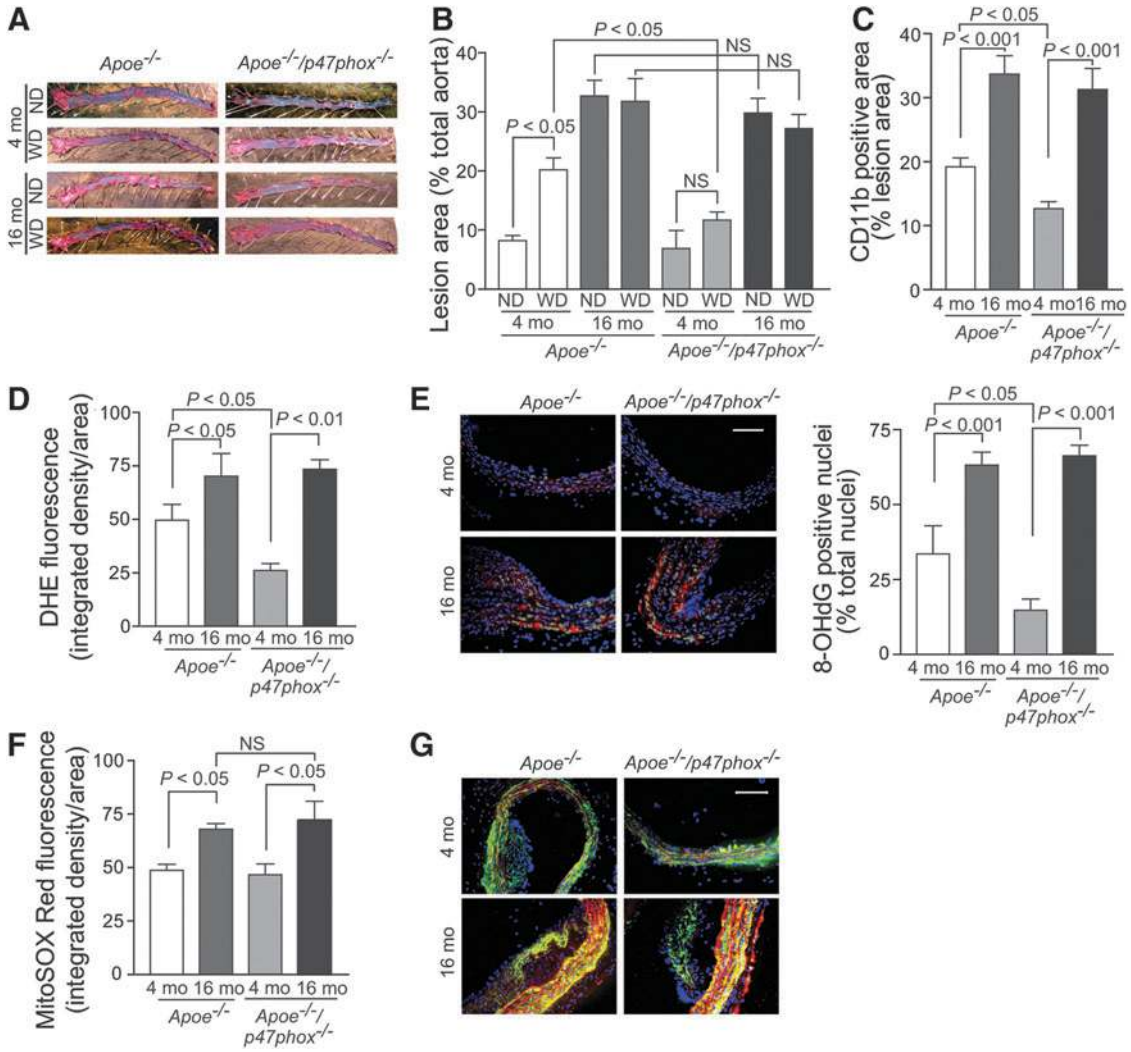

FIG. 1. Atherosclerosis burden and aortic ROS levels in young and aged *Apoe*$^{-/-}$ and *Apoe*$^{-/-}$*/p47phox*$^{-/-}$ mice. (A) Representative images of Oil Red O-stained aortas from young (4 mo) and aged (16 mo) mice fed normal chow diet (ND) and Western diet (WD) for 3 mo. Mouse aortas, perfused with PBS and fixed in 3.7% paraformaldehyde, were opened longitudinally, pinned down on black wax, stained with Oil Red O, and counterstained with 0.1% toluidine blue. **(B)** Lesion area was quantified as the percent of total aorta (mean ± SEM, $n = 15$). **(C)** Macrophage content was determined by CD11b-positive staining (mean ± SEM, $n = 8$). **(D)** Quantification of DHE fluorescence in the aortic cross sections (mean ± SEM, $n = 7$). **(E)** Representative frozen aortic cross sections stained for immunoreactive 8-hidroxy-deoxyguanosine (*red*) and counterstained with DAPI (*blue*). Nuclei positive for 8-OHdG were pseudocolored green, counted, and expressed as a percent of total nuclei. Data are presented as mean ± SEM ($n = 6$). Scale is 100 μm. **(F)** Quantification of MitoSOX Red fluorescence in the aortic cross sections (mean ± SEM, $n = 7$). **(G)** Representative fresh frozen aortic sections were stained for immunoreactive nitrotyrosine (*red*) and counterstained for smooth muscle α-actin (*green*) and with DAPI (*blue*). Scale is 100 μm. 8-OHdG, 8-hydroxy-2′-deoxyguanosine; DAPI, 4′,6-diamidino-2-phenylindole; DHE, dihydroethidium; NS, not significant; PBS, phosphate-buffered saline; ROS, reactive oxygen species; SEM, standard error of the mean.

diet had significantly lower aortic atherosclerotic lesion areas than young *Apoe*$^{-/-}$ mice ($p < 0.05$; Fig. 1A, B). However, this relationship did not hold in aging as both aged *Apoe*$^{-/-}$ and *Apoe*$^{-/-}$*/p47phox*$^{-/-}$ mice had higher atherosclerotic lesion areas, irrespective of the diet. Multiple linear regression analysis showed that age significantly increased the atherosclerotic lesion area ($r^2_{adj} = 0.45$, $p < 0.0001$), whereas *p47phox* deletion and Western diet had no effect ($p = 0.052$ and $p = 0.3$, respectively). These data suggest that *p47phox* deletion and hence lack of NOX1/2 NADPH oxidase activity, in contrast to its effect in the young, was insufficient to protect against atherosclerosis in aged *Apoe*$^{-/-}$ mice. Aging had no significant effect on cholesterol or triglyceride levels, indicating that increase in atherosclerosis with aging did not result from metabolic changes (Supplementary Table S1; Supplementary Data are available online at www.liebertpub.com/ars).

As we previously demonstrated (61), *p47phox* deletion in young *Apoe*$^{-/-}$ mice results in decreased macrophage infiltration into atherosclerotic lesions (*Apoe*$^{-/-}$*/p47phox*$^{-/-}$ 4 mo *vs. Apoe*$^{-/-}$ 4 mo, $p < 0.05$; Fig. 1C). Congruent with the increase in atherosclerotic lesion area, macrophage infiltration significantly increased with age in both *Apoe*$^{-/-}$ and *Apoe*$^{-/-}$*/p47phox*$^{-/-}$ mice ($p < 0.001$ *vs.* respective young mice), which

indicates that *p47phox* deletion had no effect on macrophage infiltration in 16 mo mice.

To assess vascular oxidative stress in these mice, we determined total ROS production in the aortic wall by staining with superoxide-sensitive indicator dihydroethidium (DHE) in fresh frozen sections (Fig. 1D). The fluorescence intensity of DHE-stained aortas was the lowest in 4 mo *Apoe*$^{-/-}$/*p47phox*$^{-/-}$ mice and was significantly higher in 4 mo *Apoe*$^{-/-}$ compared with 4 mo *Apoe*$^{-/-}$/*p47phox*$^{-/-}$ mice ($p < 0.05$). The DHE fluorescence intensity was the highest in aortas from the aged mice, and there was no difference in DHE fluorescence based on the presence or absence of *p47phox* and hence NOX1/2 NADPH oxidase activity.

To further confirm increased aortic oxidative stress with aging, fresh frozen sections were stained with 8-hydroxy-2′-deoxyguanosine (8-OHdG), an oxidative DNA damage byproduct and a surrogate marker of enhanced oxidative stress (Fig. 1E). The percent of nuclei staining for 8-OHdG was significantly higher in 4 mo *Apoe*$^{-/-}$ mice compared with the *Apoe*$^{-/-}$/*p47phox*$^{-/-}$ mice ($p < 0.05$). The percent of 8-OHdG-positive nuclei was the highest in the aortas of the aged mice ($p < 0.001$ *vs.* the young), and the 8-OHdG staining was not dependent on the presence or absence of *p47phox*, supporting the notion that NOX1/2 NADPH oxidase deletion does not result in decreased aortic ROS levels in aging.

In contrast, we observed a different pattern in regard to mtROS production. In young *Apoe*$^{-/-}$ mice, the presence or absence of NOX1/2 NADPH oxidase activity had no effect on aortic mtROS levels, as visualized by MitoSOX Red fluorescence, a mitochondria-targeted superoxide indicator. Although MitoSOX fluorescence was increased in aortas from the aged mice, *p47phox* deletion had no effect (Fig. 1F). Nitrotyrosine, which is correlated with higher mtROS levels (20), was also increased in aortic sections of both the aged *Apoe*$^{-/-}$ and *Apoe*$^{-/-}$/*p47phox*$^{-/-}$ mice, as detected by immunofluorescence (Fig. 1G). These data indicate that NOX1/2 NADPH oxidase-derived oxidative stress does not play a major role in age-dependent increase in atherosclerosis.

Aortic compliance and cardiac function are impaired with age in Apoe$^{-/-}$ *and Apoe*$^{-/-}$*/p47phox*$^{-/-}$ *mice*

To assess the potential effects of age and NOX activity on aortic stiffness, we measured aortic compliance in young and aged *Apoe*$^{-/-}$ and *Apoe*$^{-/-}$/*p47phox*$^{-/-}$ mice on chow and Western diet. In the young mice, central aortic compliance, as measured by pulse wave velocity (PWV), was similar irrespective of the diet or genotype (Fig. 2A). Aortic PWV was significantly increased in both aged *Apoe*$^{-/-}$ and *Apoe*$^{-/-}$/*p47phox*$^{-/-}$ compared with the young mice ($p < 0.05$), irrespective of the diet. However, aortic PWV was also not markedly different between normal chow and Western diet-fed aged mice. Multiple linear regression analysis showed that age significantly contributed to increase in aortic PWV in *Apoe*$^{-/-}$ mice ($r^2_{adj} = 0.21$; $p < 0.0001$), whereas *p47phox* deletion and Western diet had no effect. Blood pressure was not significantly different between young and aged *Apoe*$^{-/-}$ and *Apoe*$^{-/-}$/*p47phox*$^{-/-}$ mice, thus ruling out hypertension as a contributing factor to the increased aortic stiffening in aged mice (Fig. 2B).

We next measured the effect of age and NOX activity on cardiac function by echocardiography. Left ventricular systolic function (as measured by ejection fraction) was reduced in aged *Apoe*$^{-/-}$ and *Apoe*$^{-/-}$/*p47phox*$^{-/-}$ mice compared with the young of the same genotypes, whether on normal chow or Western diet ($p < 0.05$; Fig. 2C). Left ventricular end-diastolic volume was significantly increased in the aged mice ($p < 0.05$; Fig. 2D). Left ventricular hypertrophy (measured by left ventricle posterior wall thickness and mass) was also increased significantly in aged *Apoe*$^{-/-}$ and *Apoe*$^{-/-}$/*p47phox*$^{-/-}$ mice, independent of diet ($p < 0.05$; Fig. 2E, F). These data indicate that *p47phox* deletion does not account for age-associated cardiovascular changes.

Apoe$^{-/-}$ *and Apoe*$^{-/-}$*/p47phox*$^{-/-}$ *mice show degenerative structural changes and calcification in the aortic wall with age*

The underlying mechanisms of impaired aortic compliance may involve oxidative injury to the vessel wall (51) or mitochondrial oxidative stress-induced vascular wall remodeling in aging (66). To better understand these mechanisms, we first measured elastin and collagen content in the aortic wall of young and aged mice by histochemistry. A significant increase in collagen content was observed in the media of the aortic wall in the aged *Apoe*$^{-/-}$ and *Apoe*$^{-/-}$/*p47phox*$^{-/-}$ compared with the respective young mice ($p < 0.01$; Fig. 3A). In addition, the integrity of the elastic laminae in the media of aortas (intact in young mice) was compromised with numerous breaks in aged *Apoe*$^{-/-}$ and *Apoe*$^{-/-}$/*p47phox*$^{-/-}$ mice (Fig. 3B).

We next examined calcium deposition in the aortic sections of young and aged mice by von Kossa staining based on reports that oxidative stress induces VSMC calcification (9), and calcification is involved in aortic stiffening (40). A significant increase in calcium deposition was observed in the aortas of aged *Apoe*$^{-/-}$ and *Apoe*$^{-/-}$/*p47phox*$^{-/-}$ mice (Fig. 3C). These data indicate that p47phox-dependent NOX1/2 NADPH oxidase-derived ROS do not regulate age-associated pathological wall remodeling in the *Apoe*$^{-/-}$ mice.

Mitochondria and mitochondrial NOX4 are major sources of ROS in vascular aging

We performed several experiments to determine the source(s) of increased vascular oxidative stress in aging and to avoid confounding effects of hypercholesterolemia. We first measured superoxide and H_2O_2 levels in VSMCs isolated from young (4 mo) and aged (16 mo) wild-type and *p47phox*$^{-/-}$ mice. Consistent with our previous data (62), basal and thrombin-induced superoxide levels, as determined by 2-hydroxyethidium high-performance liquid chromatography (HPLC) analysis, were higher in aortic VSMCs from young wild-type *versus p47phox*$^{-/-}$ mice ($p < 0.01$; Fig. 4A). Basal VSMC superoxide levels increased significantly with age in both wild-type and *p47phox*$^{-/-}$ cells ($p < 0.05$ and $p < 0.001$, respectively), and superoxide levels increased significantly in response to thrombin treatment in VSMCs from both aged wild-type and *p47phox*$^{-/-}$ mice ($p < 0.05$). Similarly, basal and thrombin-induced cellular H_2O_2 levels, as determined by Amplex Red assay, were significantly increased in aged compared with young wild-type and *p47phox*$^{-/-}$ cells ($p < 0.001$; Fig. 4B). Of note, the effect of age on ROS production was independent of NOX1 NADPH oxidase activity; ROS levels were not different in VSMCs

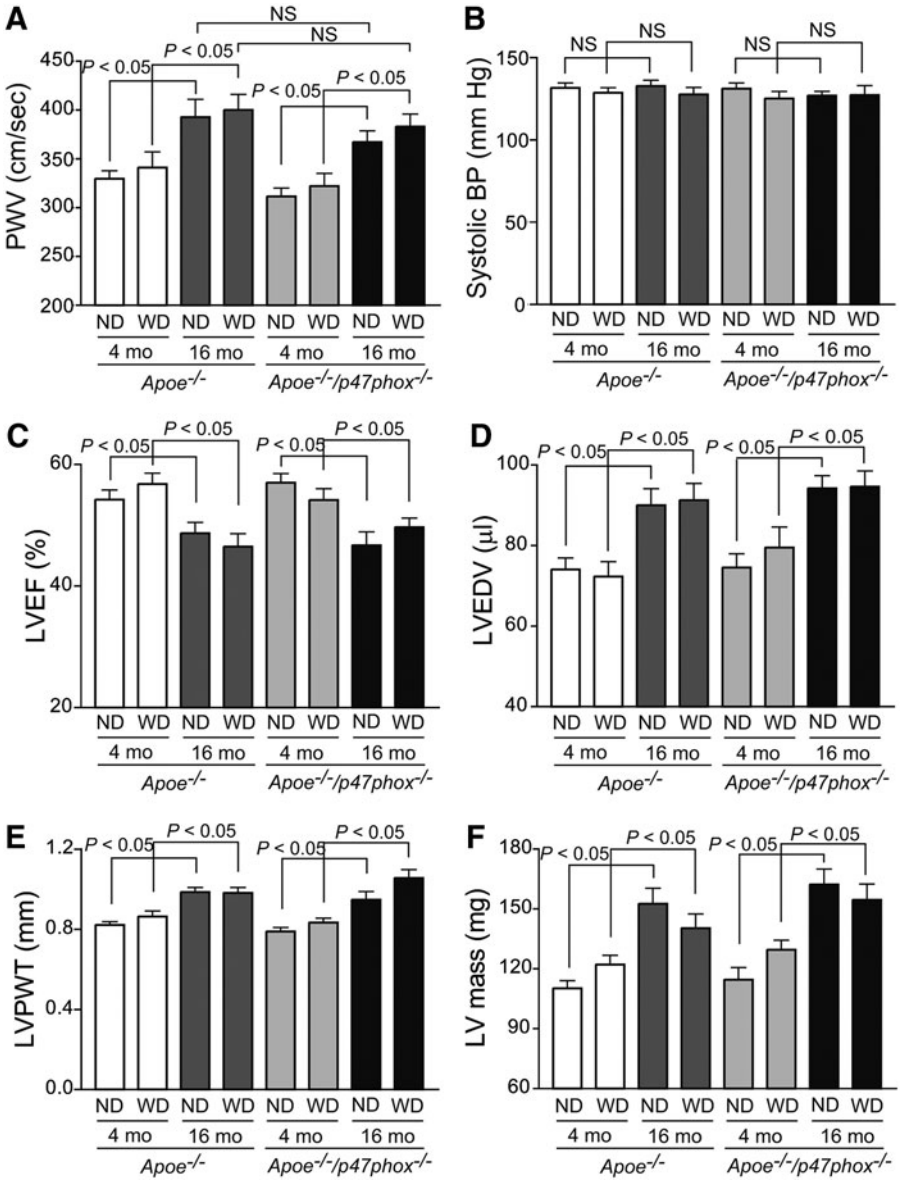

FIG. 2. Age-dependent changes in arterial compliance and cardiac function in *Apoe*$^{-/-}$ and *Apoe*$^{-/-}$*/p47phox*$^{-/-}$ mice. (A) Aortic PWV was recorded using a 20 MHz pulsed Doppler probe at the levels of the aortic arch and the abdominal aorta. Data were analyzed using the Indus Instruments Doppler Signal Processing Workstation and are presented as mean ± SEM ($n = 15$). **(B)** Systolic blood pressure was measured in conscious mice using the volume–pressure recording system (CODA 6; Kent Scientific). Data are presented as mean ± SEM ($n = 15$). Echocardiography was performed with an Ultrasound biomicroscope (Vevo 660 equipped with 30 MHz probe; VisualSonics, Inc.). Ultrasound images of the left ventricle were acquired at long axis using M-mode. LVEF **(C)**, LVEDV **(D)**, LVPWT **(E)**, and calculated LV mass **(F)** are presented as mean ± SEM ($n = 15$). LV mass, left ventricle mass; LVEDV, left ventricle end-diastolic volume; LVEF, left ventricle ejection fraction; LVPWT, left ventricle posterior wall thickness; NS, not significant; PWV, pulse wave velocity.

from aged wild-type and *p47phox*$^{-/-}$ mice either at the basal level or in response to thrombin treatment.

To identify the main source of ROS in VSMCs from aged mice, we measured superoxide and H_2O_2 levels in thrombin-treated cells pretreated with various inhibitors of ROS-generating systems (55). Oxypurinol, an inhibitor of xanthine oxidase, and nordihydroguaiaretic acid (NDGA), an inhibitor of lipoxygenase, did not decrease thrombin-induced superoxide production. Diphenyliodonium (DPI), an inhibitor of NOXs and other flavin-containing enzymes, carbonyl cyanide *m*-chlorophenylhydrazone (CCCP), an uncoupler of mitochondrial oxidative phosphorylation, and AK120765, a specific inhibitor of NOX1 and NOX4 NADPH oxidases (62), markedly decreased thrombin-stimulated superoxide levels in VSMCs from aged mice ($p < 0.05$, Fig. 4C), suggesting that both cellular NOXs and mitochondria were important sources of ROS in the aged VSMCs. In concert with that thrombin-stimulated H_2O_2 generation was significantly inhibited by DPI, CCCP, and AK120765 ($p < 0.05$, Fig. 4D). The inhibitory effects CCCP and AK120765 on thrombin-induced H_2O_2 generation were not significantly different from each other. Interestingly, AK120765 significantly reduced H_2O_2 levels at basal conditions, while CCCP did not have a significant effect (Supplementary Fig. S1).

The inhibitory effect of AK120765 is expected as NOX4 is a constitutive enzyme present in both the cytosol and mitochondria, whereas lack of significant basal H_2O_2 inhibition by CCCP might reflect natural uncoupling in aged quiescent cells (36). However, inhibitors of xanthine oxidase and lipoxygenase failed to inhibit excess H_2O_2 levels in aged VSMCs. Additional support for enhanced mtROS generation was evident from a marked increase in yellow/orange fluorescence in mitochondria, from the colocalization of MitoSOX Red and MitoTracker Green FM, in VSMCs from aged mice (Fig. 4E). To confirm that ROS generation was increased in mitochondria, we isolated mitochondria from VSMCs and measured H_2O_2 generation in the presence of citric acid cycle substrates. Mitochondria from VSMCs of aged mice had significantly increased H_2O_2

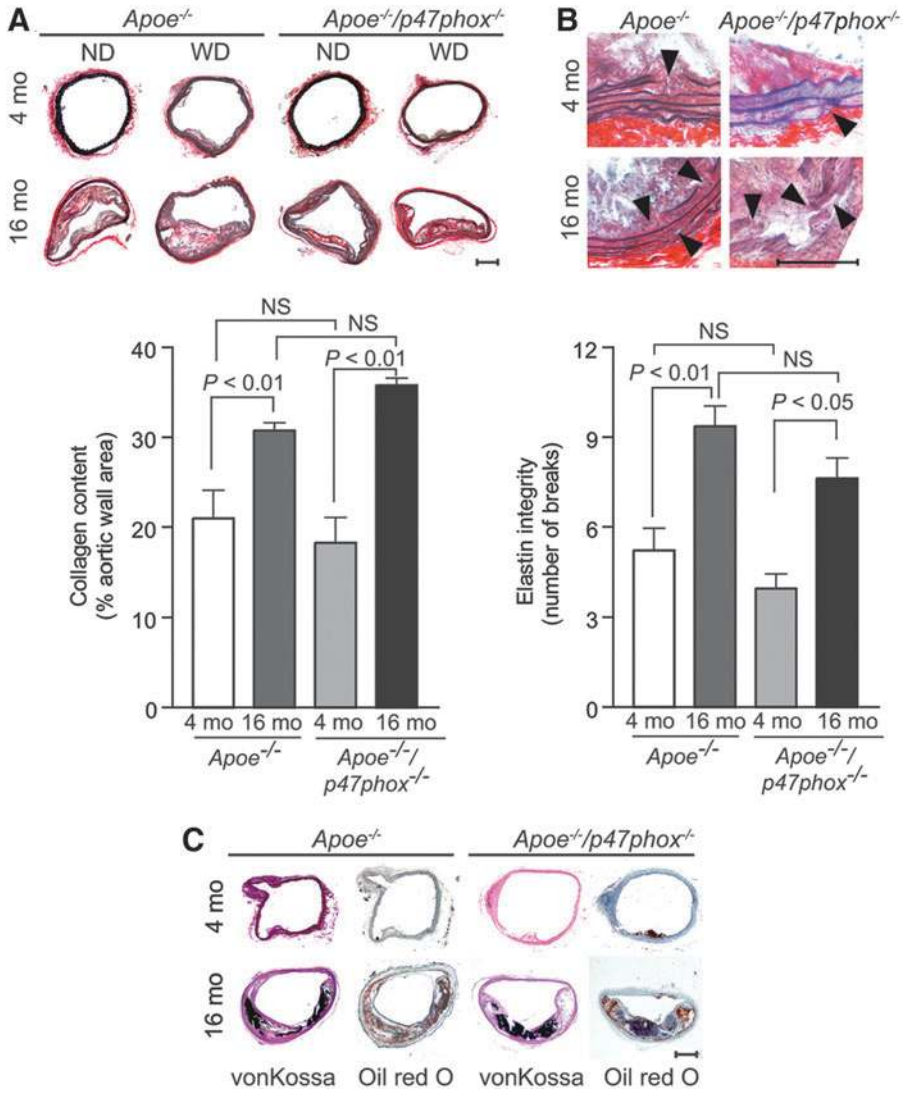

FIG. 3. Changes in aortic collagen content, elastin integrity, and calcification with age in *Apoe*$^{-/-}$ and *Apoe*$^{-/-}$*/p47phox*$^{-/-}$ mice. **(A)** Representative fresh frozen aortic sections were stained with picrosirius red (*upper panel*) and collagen content determined as the picrosirius red-positive area (mean ± SEM, $n = 10$) (*lower panel*). **(B)** Representative sections stained with Verhoeff's elastic stain (*upper panel*), with *arrowheads* showing the breaks in elastic laminae. Number of elastin laminae breaks (mean ± SEM, $n = 10$) (*lower panel*). **(C)** Representative sections were stained with von Kossa stain or Oil Red O. Scales are 100 μm. NS, not significant.

generation (Fig. 4F). Together, these data indicate that mitochondria are the major source of increased ROS in aging.

Because the inhibitory effects of DPI and AK120765 suggest that NOXs might contribute to aging-associated increase in vascular oxidative stress, NOX1/NOX2 NADPH oxidases are inactive in *Apoe*$^{-/-}$*/p47phox*$^{-/-}$ mice, and NOX4 localization in mitochondria increases mtROS levels (6), we investigated whether NOX4 is involved in aging-associated increase in ROS levels. Indeed, expression of immunoreactive NOX4 was markedly enhanced in medial and intimal SMCs in aortic atherosclerotic lesions as well as in the adventitia of aged *Apoe*$^{-/-}$ and *Apoe*$^{-/-}$*/p47phox*$^{-/-}$ mice (Fig. 5A). *Nox4* mRNA expression was also significantly increased in VSMCs isolated from aged wild-type and *p47phox*$^{-/-}$ mice ($p < 0.01$ and $p < 0.05$, respectively; Fig. 5B), and NOX4 protein levels were higher in mitochondria in VSMCs obtained from aged wild-type and *p47phox*$^{-/-}$ than in VSMCs from young mice (Fig. 5C). In contrast, NOX1 expression was minimally increased with age in mouse atherosclerotic lesions and in VSMCs from aged mice (Supplementary Fig. S2). Importantly, NOX1 was not detected in mitochondrial lysates from either young or aged VSMCs.

To determine whether increased mitochondrial NOX4 localization was actually responsible for the increased mtROS levels observed in aging, we inhibited NOX4 expression in cultured VSMCs from aged wild-type mice by transducing with lentiviral vectors containing either scrambled or *Nox4* shRNA. NOX4 protein expression was decreased in cellular as well as in mitochondrial lysates from *Nox4* shRNA-transduced cells (Fig. 5D). Mitochondrial H_2O_2 generation was significantly decreased ($p < 0.01$) in *Nox4* shRNA-transduced VSMCs from aged wild-type mice compared with scrambled shRNA-transduced or nontransduced cells (Fig. 5E). Mitochondrial H_2O_2 generation in the presence of citric acid cycle substrates was also significantly inhibited by DPI and CCCP in VSMCs from 4 mo mice ($p < 0.05$) as well as in 16 mo mice ($p < 0.001$ for DPI and $p < 0.01$ for CCCP) (Fig. 5F). AK120765 significantly inhibited mitochondrial H_2O_2 levels in VSMCs from aged, but not young, mice, which correlates with increased NOX4 expression in aged cells. Taken together, these findings suggest that increased mitochondrial NOX4 localization and NOX4 NADPH activity contribute to increased mitochondrial oxidative stress in the vasculature of aged mice.

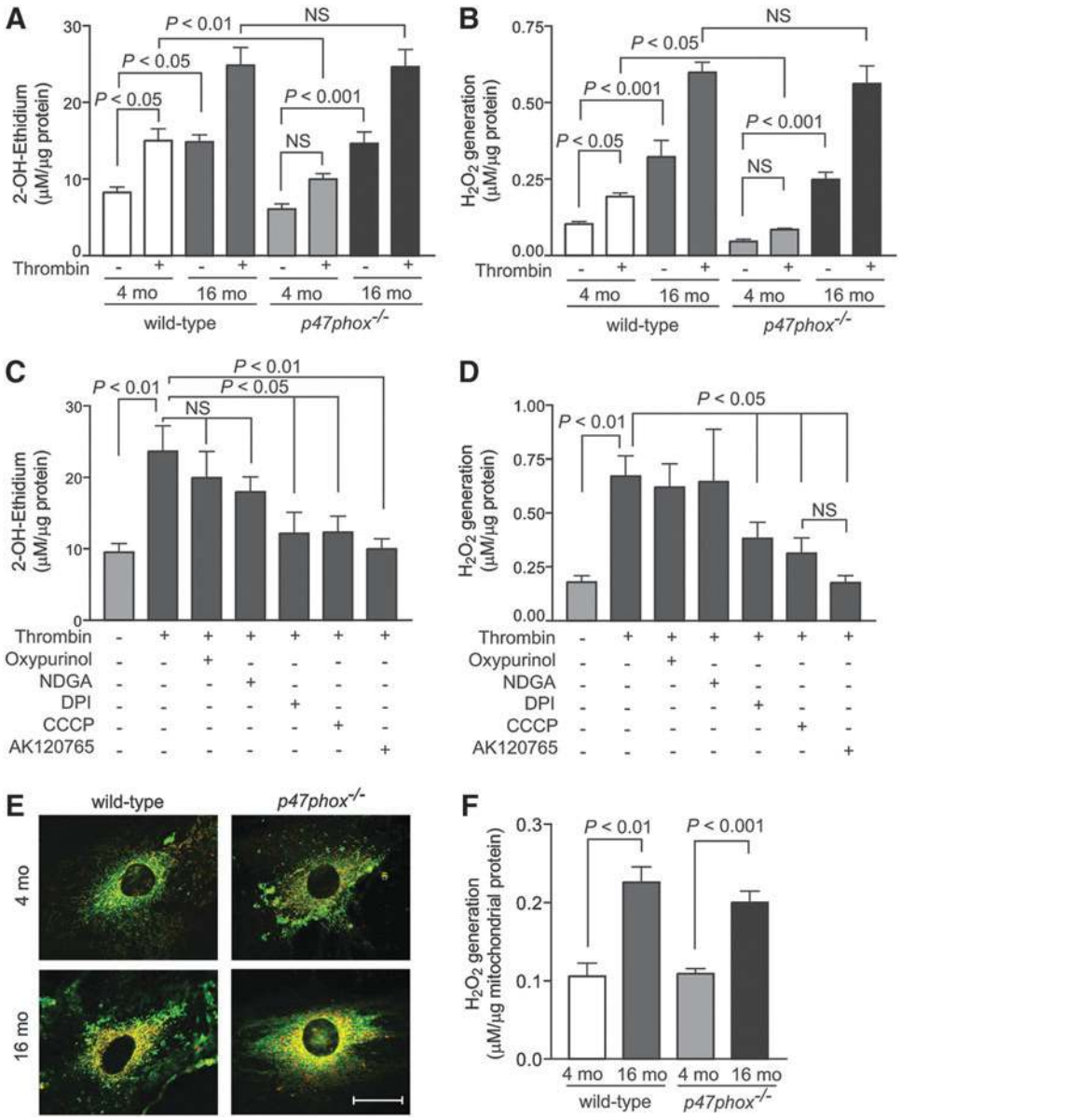

FIG. 4. Changes in total cellular and mtROS levels in aortic VSMCs of young and aged wild-type and *p47phox*$^{-/-}$ mice. VSMCs were treated with 2 U/ml thrombin for 15 min and superoxide generation was measured by 2-OH-ethidium HPLC analysis **(A)** and H_2O_2 generation was determined with Amplex Red assay **(B)**. Data are normalized to protein concentration and are the mean ± SEM of five independent experiments. VSMCs from aged wild-type mice were treated with thrombin or pretreated with 50 μM oxypurinol, 10 μM NDGA, 10 μM DPI, 2 μM CCCP, or 10 μM AK120765 for 30 min, and then treated with thrombin for 10 min. Superoxide levels were determined by 2-OH-ethidium HPLC **(C)** and H_2O_2 levels were determined with Amplex Red assay **(D)**. Data are normalized to protein concentration and are the mean ± SEM of five independent experiments. **(E)** Representative confocal microscopy images of VSMCs were stained with MitoSOX Red and MitoTracker Green FM. *Bright yellow/orange* fluorescence indicates increased ROS generation in mitochondria. Scale is 10 μm. **(F)** H_2O_2 generation by mitochondria was measured in the presence of oxidative phosphorylation substrates using Amplex Red assay. Data are the mean ± SEM of four independent experiments with duplicates. AK120765, 2-(2-chlorophenyl)-4-methyl-5-(pyridin-2-ylmethyl)-1H-pyrazolo[4,3-c]pyridine-3,6(2H,5H)-dione; CCCP, carbonyl cyanide *m*-chlorophenylhydrazone; DPI, diphenyliodonium; HPLC, high-performance liquid chromatography; mtROS, mitochondrial ROS; NDGA, nordihydroguaiaretic acid; VSMC, vascular smooth muscle cell.

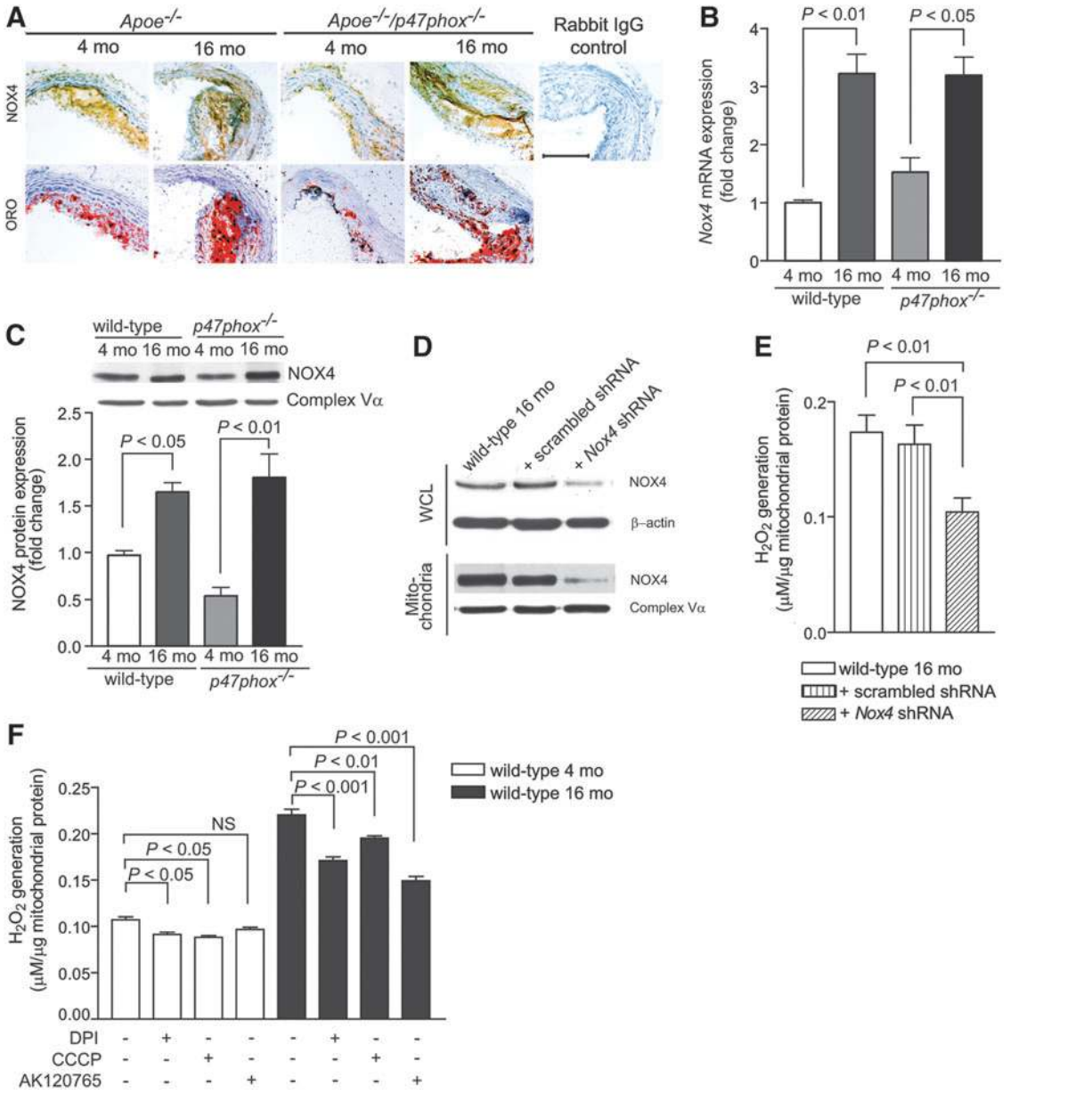

FIG. 5. Changes in NOX4 levels in atherosclerotic lesions and *Nox4* expression and NOX4 levels and function in VSMCs and VSMC mitochondria with age. **(A)** Representative aortic sections were stained for immunoreactive NOX4 and with Oil Red O. Scale is 100 μm. **(B)** Real-time reverse transcription–polymerase chain reaction analysis of VSMC *Nox4* mRNA levels. **(C)** Western blot analysis of NOX4 protein levels in VSMC mitochondria. Densitometric quantification of NOX4 levels normalized to complex Vα subunit levels. **(D)** VSMCs from aged wild-type mice were incubated with 10 multiplicity of infection (MOI) *Nox4* shRNA lentiviral particles mix (Sigma-Aldrich) in the presence of 8 mg/ml hexadimethrine bromide following the manufacturer's protocol. Successfully transduced clones were selected and further expanded using 3 μg/ml puromycin in Dulbecco's modified Eagle's medium. Control VSMCs were transduced with lentiviral nontarget shRNA particles. NOX4 levels in cells (WCL) and mitochondria were determined by Western analysis. Protein loading was normalized to β-actin in WCL and complex Vα subunit in mitochondria lysates. **(E)** H_2O_2 generation in mitochondria from lentivirus-transduced VSMCs was assayed in the presence of oxidative phosphorylation substrates using Amplex Red assay. **(F)** H_2O_2 generation in VSMC mitochondria from young and aged wild-type mice was assayed in the presence of citric acid cycle substrates and 10 μM DPI, 2 μM CCCP, or 10 μM AK120765 using Amplex Red assay. Data are the mean ± SEM, $n = 8$ **(B, C, E, F)**. NOX, NADPH oxidase; NS, not significant; WCL, whole cell lysate.

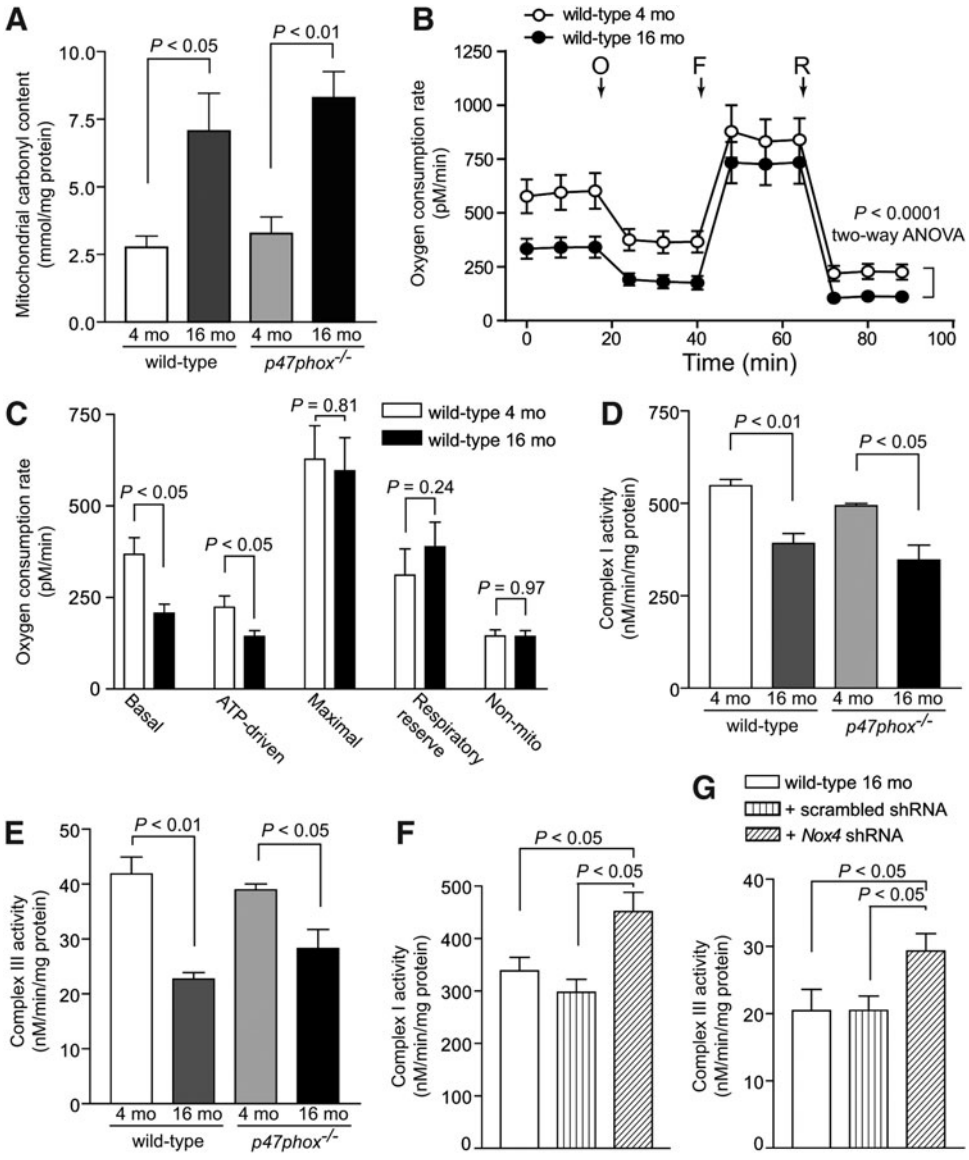

FIG. 6. Protein oxidation and mitochondrial function in VSMCs from young and aged mice and mitochondrial function in VSMCs from aged wild-type mice transduced with *Nox4* shRNA. **(A)** Mitochondrial protein carbonyl content. **(B)** Mitochondrial OCR was determined using Seahorse XF-24 analyzer. VSMCs from 4 and 16 mo mice were plated at 25,000 cells/well in XF-24 plates and OCR was measured at the basal level and in the presence of 2 μM oligomycin (O), 500 nM Trifluoromethoxy carbonylcyanide phenylhydrazone (FCCP) (F), and 500 nM rotenone (R). **(C)** Mitochondrial bioenergetic parameters were derived from the measurements of OCR in VSMCs from young and aged wild-type mice. Data are the mean ± SEM, $n = 6$ (**B**, **C**). Mitochondrial complex I **(D)** and complex III **(E)** activities in VSMCs. Mitochondrial complex I **(F)** and complex III **(G)** activities in VSMCs from aged wild-type mice transduced with lentiviral scrambled and *Nox4* shRNA. Data are the mean ± SEM of three independent experiments **(D–G)**. mo, month old; OCR, oxygen consumption rate.

Aging is associated with oxidative protein modification and mitochondrial dysfunction in VSMCs of wild-type and p47phox$^{-/-}$ mice and Nox4 knockdown improves mitochondrial function in VSMCs of aged wild-type mice

Oxidative protein carbonylation, a direct, frequent, and irreversible protein modification during oxidative stress, induces protein degradation and affects function (13, 17). To further determine the effects of increased vascular oxidative stress, we measured protein carbonylation and oxygen consumption in mitochondria isolated from VSMCs of young and aged wild-type and *p47phox*$^{-/-}$ mice. Mitochondrial protein carbonyl content was significantly increased in VSMCs from aged mice ($p < 0.05$ and $p < 0.01$ for wild-type and *p47phox*$^{-/-}$ VSMCs, respectively; Fig. 6A). The mitochondrial oxygen consumption rate (OCR), a measure of mitochondrial function determined using Seahorse XF-24 extracellular flux analyzer, was significantly lower in VSMCs from aged compared with VSMCs from young mice ($p < 0.0001$, two-way analysis of variance [ANOVA]; Fig. 6B).

Analysis of mitochondrial bioenergetic parameters showed significantly decreased basal and ATP-driven mitochondrial OCR ($p < 0.0001$), but no difference in maximal and respiratory reserve mitochondrial OCR and non-mitochondrial respiration (Fig. 6C). Activities of complex I and complex III were also decreased significantly in the mitochondria isolated from VSMCs of aged *versus* young wild-type and *p47phox*$^{-/-}$ mice ($p < 0.01$ and $p < 0.05$ for wild-type and *p47phox*$^{-/-}$ VSMCs, respectively; Fig. 6D, E). These effects were not related to NOX1 NADPH oxidase activity as there was no difference in complex activity measures between wild-type and *p47phox*$^{-/-}$ VSMCs. Importantly, mitochondrial complex I and complex III activities were significantly higher in aged wild-type cells transduced with *Nox4* shRNA lentivirus compared with scrambled shRNA-transduced and aged wild-type VSMCs ($p < 0.05$; Fig. 6F, G). Taken together, these data suggest that the increased expression/activity of mitochondrial-localized NOX4 with aging increases protein oxidation, which in turn leads to decreased activity of respiratory chain complexes,

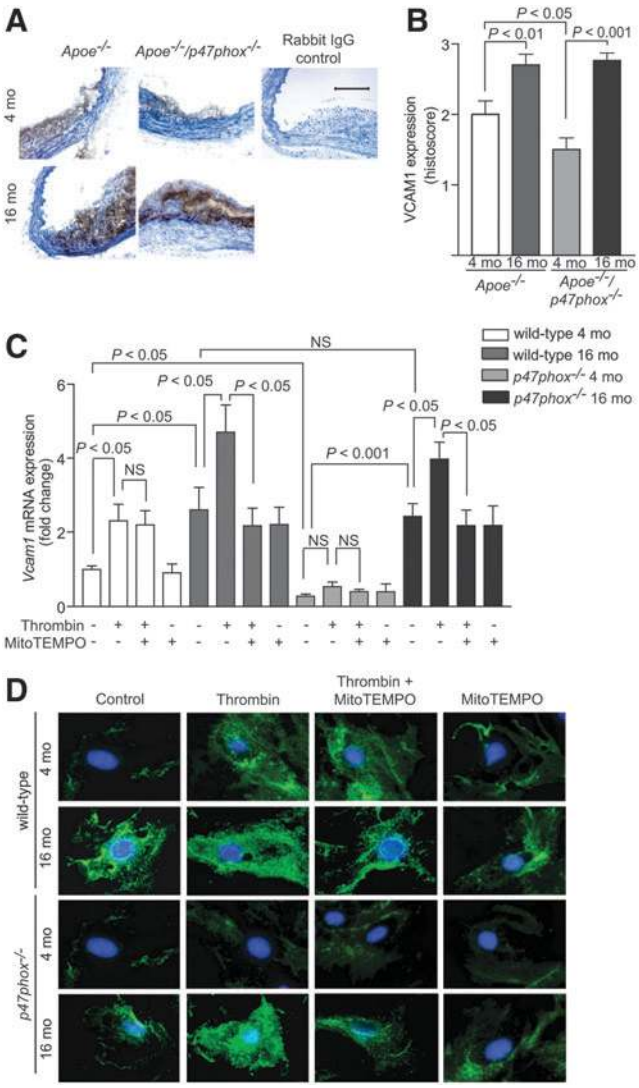

FIG. 7. Changes in mouse aortic VCAM1 protein levels with age and modulation of *Vcam1* gene expression by mtROS levels. **(A)** Representative mouse aortic sections immunostained for VCAM1. Scale is 100 μm. **(B)** Immunohistochemistry scoring of VCAM1 levels (mean ± SEM, $n = 7$). **(C)** Real-time PCR analysis of *Vcam1* mRNA expression in VSMCs of young and aged wild-type and *p47phox*$^{-/-}$ mice treated with 1 U/ml thrombin, 10 μM MitoTEMPO, and thrombin in the presence of MitoTEMPO for 4 h. Data, normalized to *18S* RNA expression and relative to the untreated wild-type 4 mo VSMCs, are the mean ± SEM of four independent experiments. **(D)** Representative images of immunofluorescent staining for VCAM1 in VSMCs of young and aged wild-type and *p47phox*$^{-/-}$ mice treated with 1 U/ml thrombin, 10 μM MitoTEMPO, and thrombin in the presence of MitoTEMPO for 16 h. MitoTEMPO, (2-(2,2,6,6-Tetramethylpiperidin-1-oxyl-4-ylamino)-2-oxoethyl)triphenylphosphonium chloride; NS, not significant; VCAM, vascular cell adhesion molecule.

impaired mitochondrial function and bioenergetics, and augmented oxidative stress in the vasculature.

Aging-associated increases in mtROS augment adhesion molecule expression in aortic wall of Apoe$^{-/-}$ *and in VSMCs of wild-type and p47phox*$^{-/-}$ *mice*

Increased mtROS production in uncoupling protein-2-deficient mice was reported to be associated with enhanced vascular cell adhesion molecule 1 (VCAM1) expression, aortic macrophage infiltration, and atherosclerosis (38). To examine the link between mtROS and vascular inflammation, we analyzed VCAM1 expression in aortic sections of young and aged *Apoe*$^{-/-}$ and *Apoe*$^{-/-}$*/p47phox*$^{-/-}$ mice. VCAM1 expression was higher in the aortas from the aged than from the young mice (Fig. 7A, B). In aged mice, VCAM1 expression was not different in aortas from *Apoe*$^{-/-}$ and *Apoe*$^{-/-}$*/p47phox*$^{-/-}$, consistent with the theme that NOX1/2 NADPH oxidases do not contribute significantly to age-associated increase in mtROS. In the young mice, however, VCAM1 expression was lower in aortas from the *Apoe*$^{-/-}$*/p47phox*$^{-/-}$ compared with the *Apoe*$^{-/-}$ mice.

In cultured cells, thrombin treatment significantly increased *Vcam1* mRNA expression in VSMCs from young wild-type, but not from young *p47phox*$^{-/-}$, mice ($p < 0.05$ for wild-type VSMCs; Fig. 7C). No difference in increase in *Vcam1* mRNA expression was observed following thrombin treatment of aged VSMCs from wild-type and *p47phox*$^{-/-}$ mice. MitoTEMPO is a combination of the antioxidant piperidine nitroxide TEMPO with the lipophilic triphenylphosphonium (TPP) cation that has a large hydrophobic surface area, which enables it to pass easily through the phospholipid bilayers and accumulate several hundred-fold within the negatively charged mitochondrial matrix (15). Treatment with 10 μM MitoTEMPO significantly inhibited thrombin-induced *Vcam1* mRNA expression in VSMCs from aged mice ($p < 0.05$), but had no effect in VSMCs from young mice (Fig. 7C). Additionally, immunofluorescence staining in VSMCs treated with thrombin showed a marked decrease in VCAM1 fluorescence in MitoTEMPO-treated cells from aged, but not young, mice (Fig. 7D). These results indicate that VSMC *Vcam1* expression is regulated by NOX1/2 NADPH oxidase-derived ROS in the young and mtROS in the aged mice, consistent with the notion that mtROS are important in sustaining and, in fact, increasing inflammation with age.

Increased NOX4 expression in aortic VSMCs of aged human subjects is associated with increased mtROS and advanced atherosclerosis

To determine the clinical relevance of our data from mouse VSMC culture experiments and aged mouse models of *Apoe* deficiency and oxidative stress, we examined NOX4 expression and mtROS generation in human aortic smooth muscle cells (HASMCs) derived from young and aged donors. *Nox4* mRNA expression was significantly increased in aged HASMCs ($p < 0.05$; Fig. 8A) and NOX4 protein expression was increased in HASMC mitochondria isolated from the aged compared with the young donors (Fig. 8B). H_2O_2 generation in the presence of oxidative phosphorylation substrates was also significantly higher in HASMC mitochondria from the aged donors ($p < 0.05$; Fig. 8C).

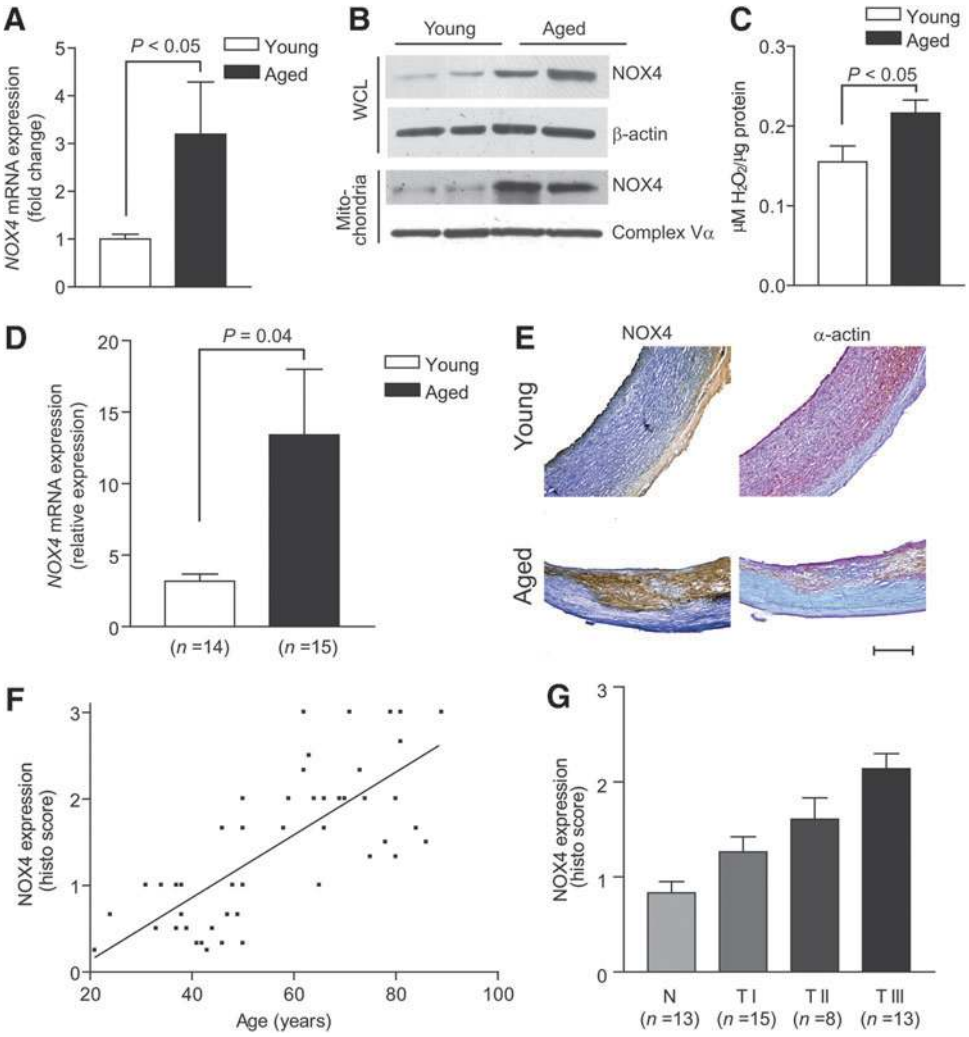

FIG. 8. NOX4 and ROS levels increase with age in HASMC mitochondria, and NOX4 levels are positively correlated with age and atherosclerotic lesion severity in human carotid arteries. **(A)** Real-time PCR analysis of *Nox4* mRNA expression in HASMCs. **(B)** Western analysis of NOX4 protein levels in mitochondria and WCLs of HASMCs. **(C)** H_2O_2 generation in HASMC mitochondria. Data are the mean ± SEM of four independent experiments in **(A)** and **(C)**. **(D)** Real-time PCR analysis of *Nox4* mRNA expression in human carotid arteries (mean ± SEM). **(E)** Representative sections of human carotid arteries were stained for immunoreactive NOX4 and smooth muscle α-actin. Scale is 500 μm. **(F)** Changes in NOX4 protein levels with age in patients ($n = 49$). **(G)** NOX4 expression increased with atherosclerotic lesion severity ($n = 49$). HASMC, human aortic smooth muscle cell.

On examination of carotid artery samples from donors of various ages, *Nox4* mRNA expression was significantly increased in the arteries from the aged compared with the young donors ($p < 0.05$; Fig. 8D). Consistent with this, immunoreactive NOX4 expression was increased in the carotid artery sections from aged donors (Fig. 8E) and correlated significantly with age ($r^2 = 0.5663$, $p < 0.0001$; Fig. 8F). Although our limited sample size precludes a definitive statement, NOX4 levels do not seem to be influenced by gender. NOX4 levels were relatively low in the initial atherosclerotic lesions (type I) and increased markedly in the early (type II) and early advanced lesions (type III) (p for trend < 0.0001; Fig. 8G). These results demonstrate a strong correlation between NOX4 levels and age-dependent atherosclerosis and, together with the observation that mitochondrial oxidative stress is increased in HASMCs from older individuals, are suggestive of a role of NOX4 in age-associated increase in atherosclerosis.

Pharmacologic inhibition of mitochondrial and NOX4 NADPH oxidase-derived ROS in aged Apoe$^{-/-}$ mice attenuated the progression of atherosclerosis and preserved aortic compliance

MitoTEMPO was shown to rapidly accumulate in the mitochondria of various tissues in mice after an IV injection (42). MitoTEMPO has been reported to decrease mitochondrial and vascular ROS levels, improve endothelial function, and protect against angiotensin II-induced hypertension in mice (15). To investigate the relevance of mitochondrial oxidative stress in aging-associated increase in atherogenesis, we treated aged *Apoe*$^{-/-}$ mice fed a Western diet with MitoTEMPO for 3 months. MitoTEMPO significantly attenuated the progression of atherosclerosis, as measured by the percent total aortic atherosclerotic lesion area, in the aged *Apoe*$^{-/-}$ compared with the vehicle-treated mice ($p = 0.01$; Fig. 9A). Total ROS levels in the aortic wall, as detected by DHE fluorescence, and mtROS, as detected by MitoSOX fluorescence, were significantly lower in the MitoTEMPO-treated compared with the vehicle-treated mice ($p = 0.025$ and $p = 0.049$ for DHE and MitoSOX fluorescence, respectively; Fig. 9B, C). Consistent with its effect on decreasing ROS levels, immunofluorescence analysis of aortic root cross sections showed that MitoTEMPO treatment significantly prevented 8-OHdG modification of DNA in the nuclei ($p = 0.02$; Fig. 9D). Congruently, plasma free 8-isoprostane levels were significantly lower in MitoTEMPO-treated mice ($p = 0.039$; Fig. 9E).

Aortic PWV and aortic wall collagen content were significantly lower in the MitoTEMPO-treated mice compared with the vehicle-treated mice, without affecting atherosclerotic

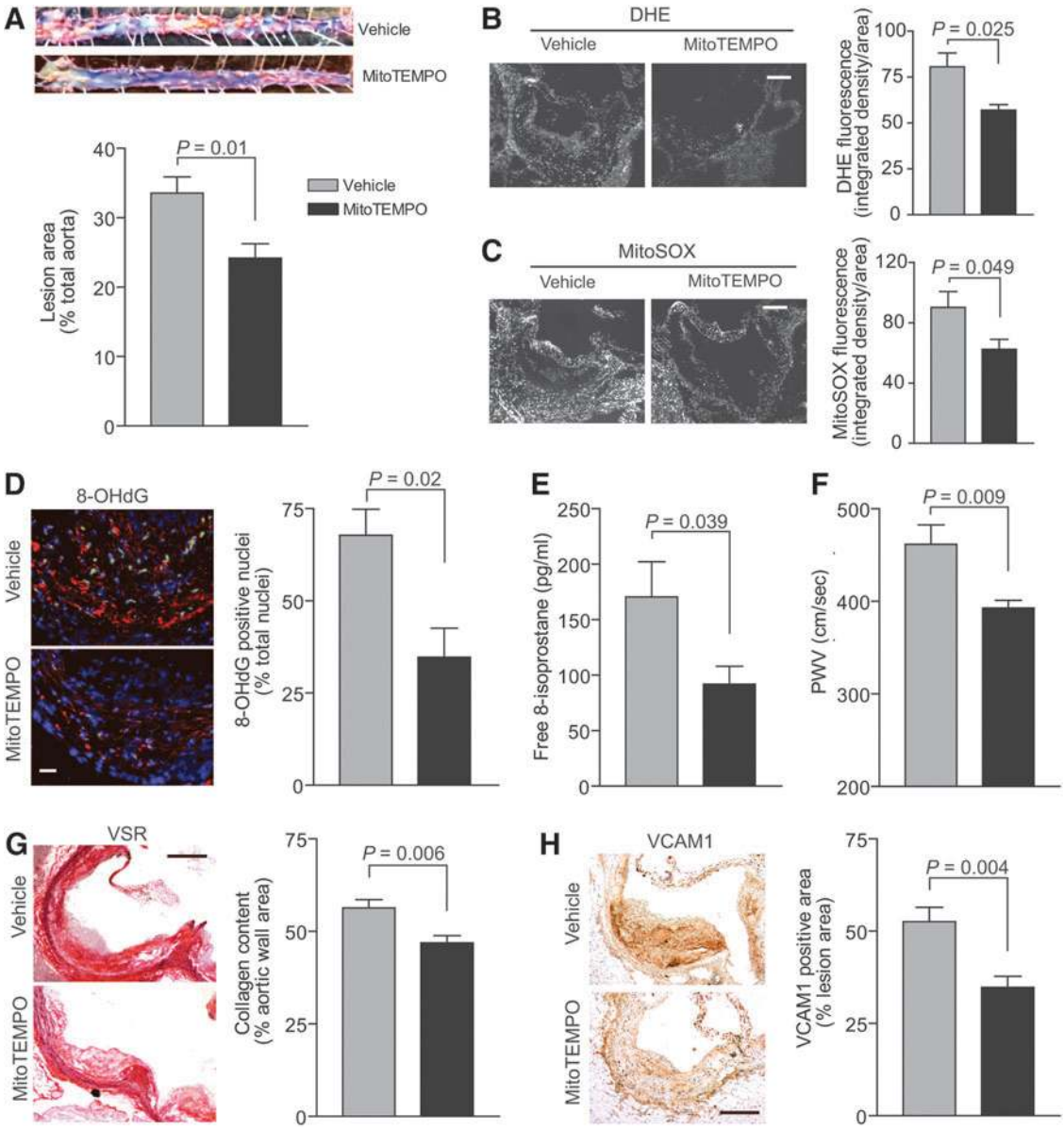

FIG. 9. MitoTEMPO treatment decreased aortic atherosclerotic lesion area and ROS levels and preserved aortic compliance in aged *Apoe*$^{-/-}$ mice. MitoTEMPO at a concentration of 1500 μg/kg/day was delivered *via* miniosmotic pumps (Alzet 1004) that were implanted subcutaneously under 1% inhaled isoflurane/O_2 anesthesia into 13 mo *Apoe*$^{-/-}$ mice. The pumps were replaced with fresh ones every 4 weeks for 12 weeks of treatment duration. The mice were fed a Western-type diet for the duration of the experiment. **(A)** Representative images and quantification of Oil Red O-stained aortas. Lesion area as percent of total aorta (mean ± SEM, $n = 8$). **(B)** Representative aortic root cross sections stained with DHE and quantification of DHE fluorescence (mean ± SEM, $n = 8$). Scale is 100 μm. **(C)** Representative sections stained with MitoSOX Red and quantification of MitoSOX Red fluorescence (mean ± SEM, $n = 8$). Scale is 100 μm. **(D)** Representative fluorescent images of aortic root sections stained for 8-OHdG (*red*) and counterstained with DAPI (*blue*). Nuclei positive for 8-OHdG were pseudocolored green, counted, and expressed as a percent of total nuclei. Data are presented as mean ± SEM ($n = 6$). Scale is 25 μm. **(E)** Free plasma 8-isoprostane levels (mean ± SEM, $n = 8$). **(F)** PWV presented as mean ± SEM ($n = 10$). **(G)** Representative aortic root sections were stained with VSR, and collagen content determined as the picrosirius red-positive area (mean ± SEM, $n = 8$). Scale is 100 μm. **(H)** Representative sections of aortic root were stained for immunoreactive VCAM1 and quantification of VCAM1 staining (mean ± SEM, $n = 8$). Scale is 100 μm. VSR, Verhoeff picrosirius red.

plaque fibrous cap integrity ($p = 0.009$ and $p = 0.006$ for PWV and collagen content, respectively; Fig. 9F, G). MitoTEMPO had no effect on immunoreactive NOX4 protein levels in the vasculature. Similar to its effect in VSMCs, MitoTEMPO treatment significantly lowered VCAM1 protein levels in the aortas of aged *Apoe*$^{-/-}$ mice ($p = 0.004$; Fig. 9H). However, MitoTEMPO treatment had no salutary effect on impaired cardiac function associated with aging in *Apoe*$^{-/-}$ mice. Plasma lipid levels were unaffected in MitoTEMPO-treated *Apoe*$^{-/-}$ mice. MitoTEMPO-treated mice did not reveal any

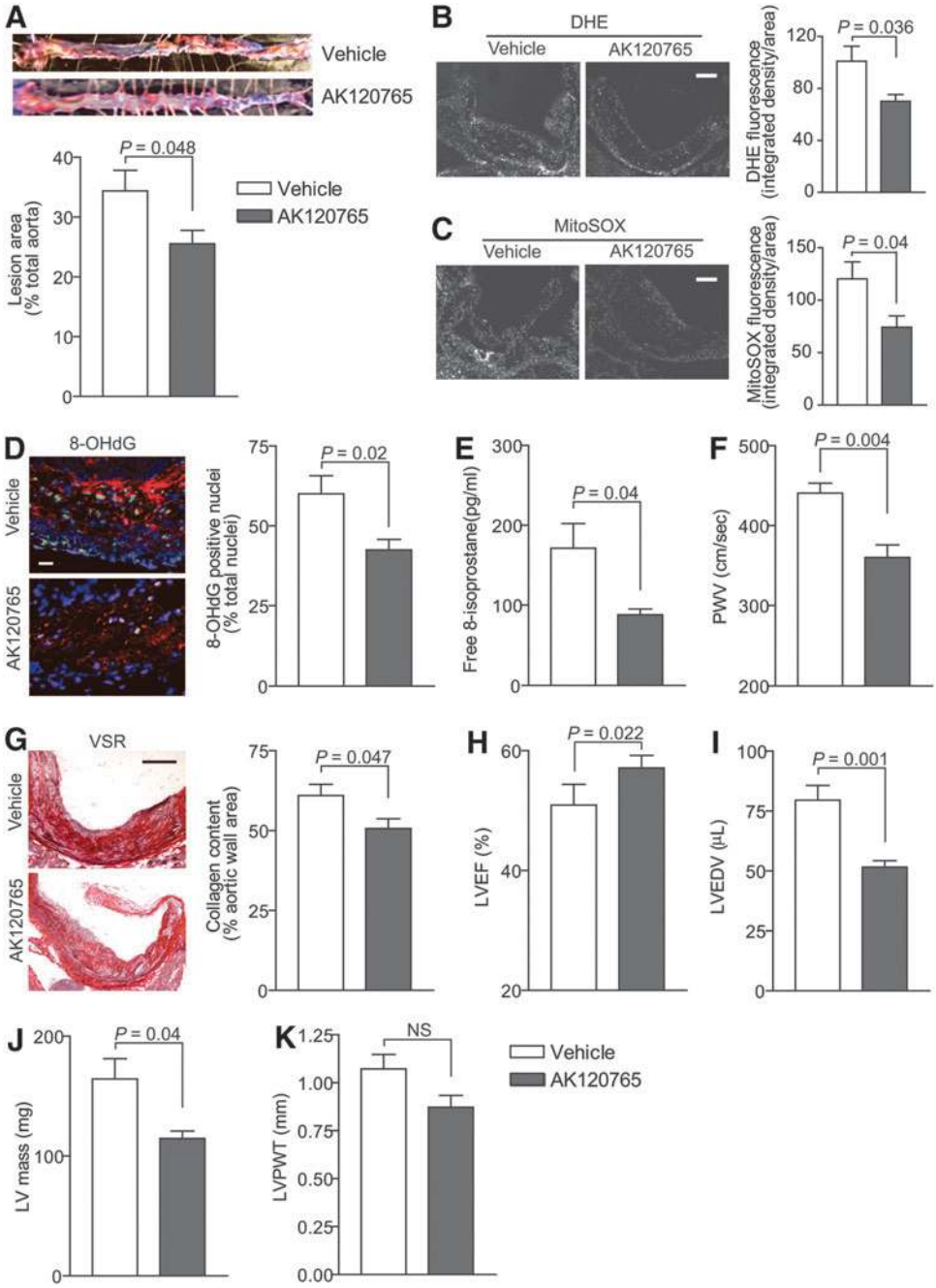

FIG. 10. AK120765 treatment lowered aortic atherosclerotic lesion area and ROS levels and preserved vascular and cardiac function in aged *Apoe*$^{-/-}$ mice. AK120765 (Ark Pharm, Inc.) was dissolved in 0.5% carboxymethylcellulose, 0.25% Tween-20, and 1% dimethyl sulfoxide at a concentration of 60 mg/kg/day and delivered by oral gavage to 13 mo *Apoe*$^{-/-}$ mice once daily for 12 weeks. The mice were fed a Western-type diet for the duration of the experiment. **(A)** Representative images and quantification of Oil Red O-stained aortas. Lesion area as a percent of total aorta (mean ± SEM, $n = 7$). **(B)** Representative aortic root cross sections were stained with DHE and quantification of DHE fluorescence (mean ± SEM, $n = 7$). Scale is 100 μm. **(C)** Representative sections stained with MitoSOX Red and quantification of MitoSOX Red fluorescence (mean ± SEM, $n = 7$). Scale is 100 μm. **(D)** Representative fluorescent images of aortic root sections were stained for 8-OHdG and counterstained with DAPI. 8-OHdG-positive nuclei were pseudocolored green, counted, and expressed as a percent of all nuclei. Data are presented as mean ± SEM ($n = 7$). Scale is 25 μm. **(E)** Free plasma 8-isoprostane levels (mean ± SEM, $n = 7$). **(F)** PWV presented as mean ± SEM ($n = 8$). **(G)** Representative aortic root sections stained with VSR and collagen content determined as the picrosirius red-positive area (mean ± SEM, $n = 7$). Scale is 100 μm. LVEF **(H)**, LVEDV **(I)**, LVPWT **(J)**, and calculated LV mass **(K)** were determined by echocardiography and are presented as mean ± SEM ($n = 7$).

overt signs of toxicity as measured by alanine aminotransferase (ALT), creatine kinase (CK), blood urea nitrogen (BUN) levels, and liver/kidney morphology (Supplementary Fig. S3). These data suggest that selective inhibition of mitochondrial oxidative stress can slow the progression of atherosclerosis and adverse vascular wall remodeling in aging.

We previously demonstrated that selective NOX1/NOX4 NADPH oxidase inhibitor AKT120765 (GKT136901) attenuated vascular ROS generation and atherosclerosis in young *Apoe*$^{-/-}$ mice (63). The GKT136901 is a specific inhibitor of NOX1/NOX4, but not NOX2 NADPH oxidase (27), and does not show inhibitory activity toward other ROS-generating and redox-sensitive enzymes (46). To assess the effect of NOX4 NADPH oxidase inhibition on ROS generation, atherosclerosis, and vascular dysfunction in aging, we treated aged *Apoe*$^{-/-}$ mice fed a Western diet for 3 months with vehicle and AK120765, a commercial preparation of GKT136901. Because NOX1 is not present in mitochondria, we used AK120765 as a chemical means to inhibit mitochondrial NOX4 NADPH oxidase activity.

Similar to our results with MitoTEMPO treatment, the percent total aortic atherosclerotic lesion area was significantly smaller in *Apoe*$^{-/-}$ treated with AK120765 compared with the vehicle-treated mice ($p = 0.048$; Fig. 10A). Aortic wall total and mtROS levels were also significantly decreased in AK120765-treated mice ($p = 0.036$ and $p = 0.04$ for DHE and MitoSOX fluorescence, respectively; Fig. 10B, C). The percent of 8-OHdG-positive nuclei in the aortic wall as well as plasma free 8-isoprostane levels were also significantly lower in AK120765-treated mice ($p = 0.02$ and $p = 0.04$ for 8-OHdG and 8-isoprostane levels, respectively; Fig. 10D, E). AK120765 had no effect on immunoreactive NOX4 protein levels in the vasculature.

Aortic stiffness was significantly lower in AK120765-treated *Apoe*$^{-/-}$ compared with the vehicle-treated mice ($p = 0.004$; Fig. 10F). Aortic wall collagen content was also significantly decreased in AK120765-treated mice ($p = 0.047$), without any changes in atherosclerotic plaque fibrous cap integrity (Fig. 10G). More importantly, aged *Apoe*$^{-/-}$ mice treated with AK120765 had higher left ventricle ejection fraction (LVEF) and lower left ventricular end-diastolic volume (LVEDV) and calculated left ventricle mass ($p = 0.022$, $p = 0.001$, and $p = 0.04$ for LVEF, LVEDV, and left ventricle mass, respectively; Fig. 10H–J), with no significant effect on left ventricle posterior wall thickness (Fig. 10K). Plasma lipid levels were unaffected in AK120765-treated *Apoe*$^{-/-}$ mice. Similar to MitoTEMPO, AK120765 did not exert any overt signs of toxicity, as measured by ALT, CK, and BUN levels and liver/kidney morphology, in aged *Apoe*$^{-/-}$ mice (Supplementary Fig. S4). These results provide further evidence that inhibition of NOX4 NADPH oxidase activity decreases mitochondrial, vascular, and systemic ROS levels, attenuates atherosclerotic burden, and preserves vascular wall and left ventricle systolic function in aging.

Discussion

The broad-ranging studies described here strongly support the hypothesis that increased mtROS, at least in part, from enhanced NOX4 expression/activity and mitochondrial localization play an important role in age-associated increase in atherosclerosis. NOX4 levels are increased in aged hyperlipidemic mice, causing increased systemic oxidative stress and inflammation. The chronic mitochondrial oxidative stress that occurs in these circumstances also induces degenerative structural changes and calcification in the aortic wall, increasing aortic stiffness and systolic dysfunction. Consistent with this, our exploratory human studies suggest a positive correlation of vascular NOX4 levels with age and atherosclerotic lesion severity. Inhibition of mtROS by MitoTEMPO and of NOX4 NADPH oxidase activity by AK120765 attenuates age-related atherosclerosis and vascular dysfunction in proatherosclerotic mice, which suggests that interventions that reduce age-related mitochondrial oxidative stress could also reduce age-associated atherosclerosis and its sequelae.

The age-dependent increase in vascular NOX4 expression observed in the current study is consistent with previous reports of similar increase in mesenteric microvasculature in humans (44) and in the murine myocardium (1). Recent studies implicate a transcriptional, post-translational, and epigenetic mechanism for regulation of NOX4 expression in senescence, a hallmark of aging and aging *per se*. Zhang *et al.* (64) reported that Nox4 expression in VSMCs is positively regulated by E2F transcription factors. In the hypophosphorylated state, retinoblastoma proteins bind E2F factors, preventing their interaction with gene promoters. It is possible that decreased cyclin-dependent kinase activity, in response to events such as increased DNA damage during aging and with increased mitochondrial oxidative stress, increases retinoblastoma protein kinase activity, consequently increasing the activity of E2F transcription factors (10).

Recently, Bai *et al.* reported that transcriptional regulation of Nox4 expression in human lung fibroblasts is mediated by an AP-1/Smad3 transcriptional complex in the far upstream promoter region of the gene (3). Post-transcriptional regulation of Nox4 in aging (60) and post-translational regulation of Nox4 in aging (14) were also reported. Finally, Sanders *et al.* (45) reported that despite its decrease at the global level, increased association of histone H4K16 in replicative senescent fibroblasts upregulates Nox4 expression, indicating an epigenetic regulation of Nox4 in aging.

Our data showed that VSMCs from aged animals display a lower basal OCR that is mostly attributed to lower ATP-driven oxygen consumption. In most cell types, ATP regeneration need is the main driver of oxygen consumption. Therefore, a lower ATP-driven OCR could either indicate a decreased ATP demand or, alternatively, reduced ability to meet cellular ATP demand due to impaired electron flow through the ETC (7). Decreased ability to meet ATP demand due to impaired ETC is less likely as maximal respiratory capacity appeared to be preserved, if not marginally increased.

An alternative hypothesis is that chronic oxidative pressure, due to increased NOX4 activity, leads to a diversion of the electrons away from the ETC toward the antioxidant systems. Interestingly, the reciprocal is also true as lower ROS levels and higher rate of NADPH regeneration were correlated with higher respiratory rates (11). Our data support this as we measured an increased H_2O_2 emission rate from the mitochondria of aged animals. Perhaps, this would constitute a feed-forward mechanism that progressively establishes a redox environment conducive to VSMC dysfunction in aging.

The age-dependent increase in *Nox4* expression and mitochondrial oxidative stress could enhance atherosclerotic

burden as increased mtROS levels induce atherogenic signaling pathways, such as those involved in endothelial dysfunction, activation, and infiltration of inflammatory cells, and endothelial and VSMC apoptosis (23). Increase in NOX4 NADPH oxidase-derived mitochondrial H_2O_2 levels may also cause a proinflammatory shift in gene expression in vascular cells *via* activation of nuclear factor-κB (58). Consistent with this notion, our results show increased mtROS-dependent VCAM1 expression in VSMCs and aortas from aged mice and also increased macrophage infiltration into atherosclerotic lesions in aged mice.

It is known that high levels of oxidized low-density lipoprotein, as is present in *Apoe*$^{-/-}$ mice, increase mtROS production by inducing SOD2 ubiquitination and degradation (53). This in turn increases mitochondrial dysfunction and mtDNA damage, resulting in hyperlipidemia and increased atherosclerosis (35). The finding that NOX4 levels are increased significantly in early, advanced human atherosclerotic lesions is in agreement with the results of Griendling and colleagues (49), which together with the observation of age-dependent increase in *Nox4* expression in the vasculature support our hypothesis that this NOX has a potential role in age-associated increase in atherogenesis.

Aortic stiffness is increased in humans (34, 59) and mice with atherosclerosis (51) and increases with age in human subjects and is an early marker of vascular dysfunction. Aged *Apoe*$^{-/-}$ and *Apoe*$^{-/-}$/*p47phox*$^{-/-}$ mice had increased mitochondrial oxidative stress and aortic stiffness similar to that previously observed by us in aged *Sod2*$^{+/-}$ mice (66), consistent with the hypothesis that mitochondrial oxidative stress is a critical determinant of central aortic compliance and is not merely a consequence of increased atherosclerosis. Of note, aortic stiffness did not increase with age in the wild-type, *p47phox*$^{-/-}$, and *Sod1*$^{+/-}$ mice (66), indicating that mitochondrial oxidative stress above a certain threshold as occurs in *Sod2*$^{+/-}$ mice or in the hypercholesterolemic background is necessary for increasing aortic stiffness. Our findings that MitoTEMPO treatment in aged *Apoe*$^{-/-}$ mice reduced vascular and systemic ROS and preserved aortic compliance through reduction of fibrotic changes in the vascular wall provide support to and insight into this potential mechanism.

Impaired endothelial function in *Apoe*$^{-/-}$ mice (16), degenerative structural changes in the aortic wall, and increased vascular inflammation in aged *Apoe*$^{-/-}$ and *Apoe*$^{-/-}$/*p47phox*$^{-/-}$ mice are all underlying factors that could induce aortic stiffening. The increased aortic calcification in the aged mice we observed is consistent with a recent report of age-dependent increase in aortic calcification in the setting of hypercholesterolemia (2). It should be noted that incubation of calcifying vascular cells with exogenous H_2O_2 enhanced Nox4 expression and promoted calcification (29).

Consistent with our data in aged *Sod2*$^{+/-}$ mice (66), increased mitochondrial oxidative stress and aortic PWV in aged *Apoe*$^{-/-}$ and *Apoe*$^{-/-}$/*p47phox*$^{-/-}$ mice are associated with impaired left ventricular function. Increased aortic PWV results in earlier return of reflected pressure wave in the late systole, which increases left ventricular afterload, causing left ventricle hypertrophy and ventricular dysfunction. In addition, increased left ventricular afterload increases the demand in cardiomyocyte contractile capacity. Emphasizing the importance of mtROS in age-dependent cardiac dysfunction, Rabinovitch and colleagues (12) reported that overexpression of mitochondria-targeted catalase attenuates murine cardiac aging and promotes longevity.

It is also likely that increased *Nox4* expression with aging is a contributing factor in cardiac dysfunction because *Nox4* overexpression in murine myocardium increases mitochondrial oxidative stress (1) and exacerbates cardiac dysfunction in response to pressure overload (26). In contrast, Shah and colleagues reported that cardiomyocyte-specific overexpression of *Nox4* protects against chronic pressure overload-induced dysfunction (65), and endothelial-specific overexpression enhances vasodilation and lowers blood pressure (43). Whether these discrepancies in NOX4 function in the cardiovascular system are related to the severity of cardiac stress and increase in NOX4 levels and/or short-term (young) *versus* long-term (aged) *Nox4* expression remains to be determined.

Of the NOXs, NOX4 is unique in that it generates mostly H_2O_2 (41). NOX4-derived H_2O_2 may be an active participant in signaling in both acute conditions because of the K_m of NOX4 for O_2 and in chronic conditions, which induce *Nox4* expression. Lending support to the plausible role of mitochondrial NOX4-derived H_2O_2 in cardiovascular pathophysiology, SOD1 activity-dependent mitochondrial-derived H_2O_2 is considered an important factor in inducing cellular dysfunction and fibrosis (19, 21). In addition, the action of NOX4 might be contextual as Thannickal *et al.* (56) reported that NOX4 exerts an antagonistic pleiotropic action such as myofibroblast differentiation and wound healing, a beneficial effect, in young subjects, but a persistent fibrosis, a detrimental effect, in the aged.

The use of small-molecule inhibitors of NOX4 was recently shown to be effective in preventing fibrosis of the liver and kidney, as well as aging-associated pulmonary fibrosis (22, 24, 46). Our data support the notion that inhibition of VSMC NOX4 prevents the adverse structural changes in the vascular wall with aging, although NOX4 inhibition in the endothelial cells and fibroblasts may also have a salutary effect on vascular function. While we cannot completely exclude the effects of NOX1 inhibition by AK120765, our data that MitoTEMPO has similar effects in aged *Apoe*$^{-/-}$ mice suggest that attenuation of mitochondrial dysfunction and oxidative stress, decrease in atherosclerosis progression, reduction of pathological vascular wall remodeling, and preservation of cardiac systolic function result from the inhibition of NOX4.

In summary, our results suggest that NOX4, but not NOX1/2, NADPH oxidase is a critical mediator of increased mitochondrial oxidative stress, vascular inflammation and dysfunction, and progression of CVD during aging. Inhibition of mitochondrial oxidative stress and dysfunction, either by targeting NOX4 activity/expression or by using mitochondrial antioxidants, may offer therapeutic potential for the prevention and treatment of age-related CVD.

Materials and Methods

Animals

Male wild-type, *p47phox*$^{-/-}$, *Apoe*$^{-/-}$, and *Apoe*$^{-/-}$/*p47phox*$^{-/-}$ mice were on the C57BL/6J background. Mice were purchased from the Jackson Laboratory and bred in-house. Littermates from heterozygous breeders were used in all the experiments. Mice were housed at 22°C with a 12-h

light/12-h dark cycle, with free access to food and water. Mice were fed standard rodent chow until 1 month (young) or 13 months of age (aged) and then a Western-type diet (Harlan Teklad #88137) for an additional 3 months.

MitoTEMPO (VDM Biochemicals, LLC) at a concentration of 1500 μg/kg/day was delivered *via* miniosmotic pumps (Alzet 1004; Durect) that were implanted subcutaneously under 1% inhaled isoflurane/O_2 anesthesia. The pumps were replaced with fresh ones every 4 weeks for 12 weeks of treatment duration. AK120765 (Ark Pharm, Inc.) was dissolved in 0.5% carboxymethylcellulose, 0.25% Tween-20, and 1% dimethyl sulfoxide at a concentration of 60 mg/kg/day and delivered through oral gavage once daily for 12 weeks (63). Mice were randomly assigned to either drug or vehicle-receiving group. Both groups were housed together in the cages to avoid environmental bias. All procedures were performed in compliance with protocols approved by the University of North Carolina Institutional Animal Care and Use Committee in accordance with NIH guidelines.

SMC isolation and culture

VSMCs were isolated from aortas of 4 or 16 mo wild-type and p47phox$^{-/-}$ mice. Briefly, aortas were dissected, cleaned, and incubated in collagenase type II at 37°C to remove adventitia and endothelium, and then digested in collagenase type II and elastase at 37°C for 1 h. Mouse VSMCs were cultured in Dulbecco's modified Eagle's medium (DMEM) supplemented with 10% fetal bovine serum (FBS) and an antibiotic/antimycotic solution. All experiments were performed using VSMCs between passages 3 and 11 that were growth arrested for 72 h in DMEM supplemented with 0.1% FBS. In the mtROS and function measurement experiments, cells were growth arrested in 0.1% FBS DMEM overnight. HASMCs, isolated from normal aortas of young (19.6 ± 0.5 years old) and aged (62 ± 2 years old) donors, were purchased from Lonza, Inc., Cell Applications, Inc., and Lifeline Cell Technology, LLC. Cells were grown in SmGM-2 medium supplemented with growth factors (Lonza). Experiments were performed using HASMCs between passages 2 and 8.

Lentiviral Nox4 shRNA

Lentiviral transduction particles containing shRNA targeting mouse *Nox4* were purchased from Sigma-Aldrich. Five different clones were used simultaneously (TRCN0000076583, TRCN0000076584, TRCN0000076585, TRCN0000076586, and TRCN0000076587). VSMCs were incubated with 10 multiplicity of infection (MOI) lentiviral particles mix in the presence of 8 mg/ml hexadimethrine bromide following the manufacturer's protocol. Successfully transduced clones were selected and further expanded using 3 μg/ml puromycin in DMEM. Control VSMCs were transduced with lentiviral nontarget shRNA control particles (Sigma-Aldrich).

Human carotid arteries

Snap-frozen carotid artery segments collected during autopsy 10–12 h postmortem were obtained through National Disease Research Interchange. Carotid artery samples were collected during endarterectomy procedures at St. Thomas' Hospital under informed consent. Donors ranged in age from 21 to 89 years, with an average age of 57 ± 18 years. There were nine female and 40 male donors. All human samples were deidentified and their use was approved by the University of North Carolina Institutional Review Board.

Arterial compliance, echocardiography, and blood pressure measurement

Arterial compliance was determined as described previously (66). Briefly, mice were anesthetized by inhalation of 1% isoflurane/O_2 mixture and fixed in the supine position on the temperature-controlled electrocardiography (ECG) board (THM 100; Indus Instruments). Body temperature was monitored with a rectal probe and maintained at 37°C. Blood flow velocity was recorded using a 20 MHz pulsed Doppler probe at the levels of the aortic arch and the abdominal aorta. Data were analyzed using the Indus Instruments Doppler Signal Processing Workstation. Aortic PWV was calculated by dividing the distance between the points at the aortic arch and abdominal aorta (40 mm), used for blood flow velocity measurements, by difference in pulse wave arrival time in respect to ECG R-peaks.

Echocardiography was performed with an Ultrasound biomicroscope (Vevo 660 equipped with 30 MHz probe; VisualSonics, Inc.) as described previously (66). Mice were anesthetized by inhalation of 1% isoflurane/O_2 mixture and fixed in the supine position on the ECG temperature-controlled board. Ultrasound images of the left ventricle were acquired at long axis using M-mode. Measurements of the interventricular septum, posterior wall thickness, and ventricle internal diameter at systole and diastole were made. Ejection fraction, end-diastolic volume, and myocardial mass were derived using VisualSonics Vevo 660 software.

Systolic blood pressure was measured in conscious mice using the volume–pressure recording system (CODA 6; Kent Scientific) as described previously (66).

Histology, immunostaining, and Western blot analysis

Mouse aortas, perfused with phosphate-buffered saline (PBS) and fixed in 3.7% paraformaldehyde, were opened longitudinally, pinned down on black wax, stained with Oil Red O, and counterstained with 0.1% toluidine blue. To make fresh frozen sections, mouse aortas were perfused with PBS, dissected, embedded in Tissue-Tek O.C.T. Compound (Sakura Finetek), and snap-frozen in liquid nitrogen. Transverse serial sections of 15 μm thickness were cut from the aortic arch, thoracic, and abdominal segments. Frozen sections were stained with Oil Red O, Verhoeff-picrosirius red, or by the von Kossa method. Digital images of stained aortic sections were analyzed with NIH ImageJ. Collagen content was measured as the picrosirius red-positive area in the aortic wall.

For immunohistochemistry, mouse aortic or human carotid artery sections were fixed in acetone and blocked in 0.3% H_2O_2 in methanol. Sections were immunostained with rabbit anti-Nox4 and anti-α-smooth muscle actin (SMA; Abcam), anti-VCAM1 (CD106) (BD Pharmingen), and anti-CD11b (Abnova) using the VECTASTAIN Elite ABC Kit and Vector DAB or Vector NovaRED Substrate Kit (Vector Laboratories, Inc.). For immunofluorescence, frozen mouse aortic sections were fixed in cold methanol, permeabilized

in 0.1% Triton X-100, and incubated with goat anti-8-hydroxyguanosine (Thermo Scientific) and AlexaFluor 568 rabbit anti-goat IgG (Life Technologies) or rabbit anti-nitrotyrosine Cy3-conjugated (Bioss, Inc.) and anti-SMA fluorescein iosthiocyanate-conjugated (Sigma-Aldrich) antibodies. Sections were mounted in Vectashield mounting medium for fluorescence with 4′,6-diamidino-2-phenylindole (Vector Laboratories). Images were acquired with a Nikon Eclipse E800 microscope at the same photomultiplier tube voltage, exposure, gain, and offset.

Plaque cellular composition was determined as CD11b and α-SMA-positive percentage of lesion area. Numerical immunohistochemistry scoring (1—weak; 2—moderate; 3—strong staining intensity) was used to determine the protein expression. Carotid atherosclerotic lesions were graded according to the American Heart Association atherosclerotic lesions classification (50). The histological scoring and atherosclerotic lesion grading were confirmed by a second independent observer blinded to the initial scores.

Western blot analysis was performed as described previously (61). Briefly, total protein from VSMCs was extracted using M-PER Mammalian Protein Extraction Reagent supplemented with Halt Protease Inhibitor Cocktail (Thermo Scientific). Cell lysates were cleared by centrifugation at 16,000 *g* for 10 min at 4°C. Protein concentration was determined using Bio-Rad protein assay. Equal amounts of protein lysates were resolved on 10% sodium dodecyl sulfate–polyacrylamide gel electrophoresis, then transferred to the nitrocellulose membrane. After washing and blocking in 5% nonfat milk in TBST, membranes were incubated with primary antibody, and then with matching secondary horseradish peroxidase-labeled antibody. Primary antibodies used were anti-NOX4 (Abcam), anti-complex V-α (MitoSciences), and anti-β-actin (Sigma-Aldrich). Using enhanced chemiluminescence reagent (Denville Scientific), antigen–antibody complexes were visualized on X-ray film. The intensity of the bands was determined by densitometry using Image Quant software (GE Healthcare).

Aortic, intracellular, and mtROS detection

Measurements of ROS in cultured cells were performed immediately after sample collection. Tissue samples were snap-frozen in liquid nitrogen, embedded in OCT, and stored at −80°C immediately after dissections. Frozen blocks were sectioned with cryotome and the sections were analyzed for ROS levels immediately after sectioning. Plasma samples were snap-frozen and stored at −80°C in gastight cryovials immediately after collection. All samples were processed within a week after collection. Incubation of cross sections with ROS detectors was performed in nitrogen-enriched atmosphere. Several negative and positive controls were used in the assays to ensure specificity and accuracy of the measurements.

DHE and MitoSOX Red fluorescence are indirect measures of superoxide levels (61). The presence of hexyl-TPP cation in MitoSOX increases its mitochondrial accumulation. Fresh frozen aortic sections were incubated with 10 μM DHE or 5 μM MitoSOX Red (Invitrogen) in the presence or absence of 200 U/ml SOD–polyethylene glycol (PEG-SOD; Sigma-Aldrich) in Hank's balanced salt solution containing 1 mM $CaCl_2$ and 1 mM $MgSO_4$ (HBSS/Ca/Mg) at 37°C for 15 min. DHE and MitoSOX Red fluorescence images were acquired with an Olympus FV500 confocal laser scanning microscope or Nikon Eclipse E800, using 510 nm excitation/580 nm emission filters at the same photomultiplier tube voltage, exposure, gain, and offset. Images were converted to grayscale and the integrated density per image area of interest was measured using NIH ImageJ 1.43. Background fluorescence from PEG-SOD-treated controls was subtracted to determine final DHE and MitoSOX Red fluorescence values.

In cell culture experiments, H_2O_2 generation was measured using the Amplex® Red Hydrogen Peroxide Assay Kit (Invitrogen) according to the manufacturer's protocol. Fluorescence was read at 530 nm excitation and 590 nm emission using the Wallac 1420 VICTOR2 Multilabel plate reader (PerkinElmer). The H_2O_2 levels were determined after background subtraction from PEG-catalase-treated controls and based on an H_2O_2 standard curve. The levels of superoxide generation were assessed with HPLC-based detection of 2-hydroxyethidium as described by Zielonka *et al.* (67). Briefly, VSMCs were incubated with 50 μM of DHE (Invitrogen), harvested in acetonitrile, sonicated, centrifuged, and the supernatants dried under vacuum. Dried pellets were stored at −20°C in the amber gastight vials. Samples were analyzed on the Agilent 1100 HPLC system using Partisil 5 μ ODS(3) column, 250 × 4.6 mm (Phenomenex). Quantification was performed based on the 2-hydroxyethidium standard curve (Noxygen Science Transfer and Diagnostics GmbH).

For mtROS detection, VSMCs grown in glass-bottom plates were washed with HBSS/Ca/Mg and incubated with 5 μM MitoSOX Red and 100 nM MitoTracker Green FM (Invitrogen) at 37°C for 15 min. Confocal images were acquired with an Olympus FV500 confocal laser scanning microscope using 510 nm excitation/580 nm emission filters for MitoSOX Red and 490 nm excitation/510 nm emission filters for MitoTracker Green FM at the same photomultiplier tube voltage, exposure, gain, and offset. Mitochondria were isolated from VSMCs of 4 and 16 mo wild-type and *p47phox*$^{-/-}$ mice using the Mitochondria Isolation Kit for Cultured Cells (Thermo Scientific), and H_2O_2 generation in isolated mitochondria in the presence of citric acid cycle substrates—5 mM sodium glutamate, 5 mM malate, and 10 mM succinate—was assessed with the Amplex Red Hydrogen Peroxide Assay Kit (Invitrogen) according to the manufacturer's protocol. The buffer contained 125 mM KCl, 2 mM KH_2PO_4, 5 mM $MgCl_2$, 10 mM ethylene glycol tetraacetic acid, and 5 mM HEPES at pH 7.2. Background fluorescence from PEG-catalase-treated controls was subtracted to determine final H_2O_2 levels.

Mitochondrial function

Mitochondrial bioenergetics was evaluated using the Seahorse XF-24 extracellular flux analyzer (Seahorse Biosciences). VSMCs isolated from aortas of 4 and 16 mo wild-type mice were maintained in DMEM supplemented with 10% FBS and 1% antibiotic/antimitotic solution and used at passages 6 or 7. Before the experiments, four replicates of cells of each age were seeded in XF24 plates at 25,000 cells per well and grown for 24 h. At 1 h before the measurements, the growth medium was replaced with the experimental medium constituted of unbuffered DMEM containing 10 mM glucose, 4 mM glutamine, and 2 mM pyruvate. Basal OCR was quantified by three consecutive cycles, in which

continuous oxygen consumption was measured for 3 min. Basal mitochondrial respiration was calculated by subtracting OCR in the presence of 500 n*M* rotenone, a respiratory chain inhibitor. ATP regeneration-driven OCR was calculated by subtracting OCR in the presence of 2 μM oligomycin, an ATP synthase inhibitor. Maximal respiration, an index of spare respiratory capacity, was quantified in the presence of 500 n*M* Trifluoromethoxy carbonylcyanide phenylhydrazone (FCCP), a chemical proton ionophore that uncouples the respiration rate from ATP regeneration rate. Finally, respiratory reserve capacity was calculated by subtracting basal OCR from maximal OCR.

Mitochondrial complex I activity was measured using Enzyme Activity Microplate Assay Kits (Abcam) following the manufacturer's protocol. Briefly, isolated mitochondria were lysed and equal amounts of protein were incubated on a microplate coated with complex I capture antibody. Complex I activity was determined by measuring reduction of NADH-sensitive Epsilon dye at 450 nm. Mitochondrial complex III activity was measured as described by Luo *et al.* (30). Briefly, isolated mitochondria were incubated with decylubiquinol and cytochrome *c* at 30°C. Complex III activity was determined by following the reduction of cytochrome *c* at 550 nm. Antimycin A-specific activity was subtracted from the total activity to calculate complex III-specific activity.

Mitochondrial protein carbonyl content

Mitochondrial protein carbonyl concentration was measured using the Protein Carbonyl Assay Kit (Cayman Chemical Company) according to the manufacturer's protocol. The assay utilizes the reaction between 2,4-dinitrophenylhydrazine and protein carbonyls, which results in formation of Schiff base to produce corresponding protein hydrazone that can be analyzed spectrophotometrically. To prevent erroneous contribution of nucleic acids to higher estimation of carbonyl content, samples were incubated with 1% streptomycin sulfate before the assay.

RNA extraction and real-time reverse transcription–polymerase chain reaction

Total RNA from VSMCs was extracted using the RNeasy Micro Kit (Qiagen, Inc.). Reverse transcription was performed with 5 μg of total RNA using the TaqMan Reverse Transcription Reagent Kit (Applied Biosystems). Real-time reverse transcription–polymerase chain reaction was carried out using the Applied Biosystems 7900 HT Sequence Detection System and TaqMan PCR Master Mix and TaqMan Gene Expression Assays for mouse *Nox1* (Mm00549170_m1), *Nox4* (Mm00479246_m1), *p22phox* (Mm00514478_m1), *Vcam1* (Mm00449197_m1), *18S* (Hs9999901_s1), and human *NOX4* (Hs00418356_m1) (Applied Biosystems). The data for each gene were analyzed using REST2009. Relative expression of each gene was determined by normalization to *18S* ribosomal RNA expression.

Plasma sample collection, clinical biochemistry tests, and 8-isoprostane enzyme immunoassay

Plasma samples were collected from deeply anesthetized mice as described previously (63). Plasma cholesterol, triglycerides, glucose, ALT, creatinine kinase MB, creatinine, and blood urea nitrogen were measured on an Automated Chemical Analyzer (Johnson & Johnson; VT350) at the UNC Animal Clinical Chemistry Laboratory. Plasma free 8-isoprostane was measured with the EIA Kit (Cayman Chemical) following the manufacturer's protocol. Because lipid levels in measured samples were not different, only the free plasma 8-isoprostane was measured.

Statistical analyses

All data sets were tested for normality using normal quantile plots and the Kolmogorov–Smirnov test. All analyses were performed using Prism, InStat software (GraphPad Software, Inc.), or SPSS v.17. Results for the atherosclerotic lesion size, PWV, and cardiac function measurements were analyzed for homogeneity variances using Levene's test and data were transformed using a square root, logarithm, or a reciprocal square root transformation in succession until the test for homogeneity was no longer reaching significance. Transformed data were analyzed by one-way ANOVA with *post hoc* multiple comparisons using the Ryan–Einot–Gabriel–Welsch F test for homogeneous subsets.

Other quantitative data were analyzed by one-way ANOVA with *post hoc* analysis using the Newman–Keuls test. Atherosclerosis and PWV data were analyzed by multiple linear regression tests with age, type of diet, and genotype as independent variables. Results from MitoTEMPO- and AK120765-treated mice were analyzed by unpaired two-tailed *t*-test. The relationship between NOX4 levels and age was analyzed using Pearson correlation. Differences were considered significant at $p < 0.05$.

Acknowledgment

This work was supported, in part, by NIH grants, AG024282, HL111664, and TR000083.

Author Disclosure Statement

No competing financial interests exist.

References

1. Ago T, Kuroda J, Pain J, Fu C, Li H, and Sadoshima J. Upregulation of Nox4 by hypertrophic stimuli promotes apoptosis and mitochondrial dysfunction in cardiac myocytes. *Circ Res* 106: 1253–1264, 2010.
2. Awan Z, Denis M, Bailey D, Giaid A, Prat A, Goltzman D, Seidah NG, and Genest J. The LDLR deficient mouse as a model for aortic calcification and quantification by micro-computed tomography. *Atherosclerosis* 219: 455–462, 2011.
3. Bai G, Hock TD, Logsdon N, Zhou Y, and Thannickal VJ. A far-upstream AP-1/Smad binding box regulates human NOX4 promoter activation by transforming growth factor-β. *Gene* 540: 62–67, 2014.
4. Ballinger SW, Patterson C, Knight-Lozano CA, Burow DL, Conklin CA, Hu Z, Reuf J, Horaist C, Lebovitz R, Hunter GC, McIntyre K, and Runge MS. Mitochondrial integrity and function in atherogenesis. *Circulation* 106: 544–549, 2002.
5. Barry-Lane PA, Patterson C, van der Merwe M, Hu Z, Holland SM, Yeh ET, and Runge MS. p47phox is required for atherosclerotic lesion progression in ApoE(–/–) mice. *J Clin Invest* 108: 1513–1522, 2001.

6. Block K, Gorin Y, and Abboud HE. Subcellular localization of Nox4 and regulation in diabetes. *Proc Natl Acad Sci U S A* 106: 14385–14390, 2009.
7. Brand MD and Nicholls DG. Assessing mitochondrial dysfunction in cells. *Biochem J* 435: 297–312, 2011.
8. Brandes RP, Weissmann N, and Schroder K. NADPH oxidases in cardiovascular disease. *Free Radic Biol Med* 49: 687–706, 2010.
9. Byon CH, Javed A, Dai Q, Kappes JC, Clemens TL, Darley-Usmar VM, McDonald JM, and Chen Y. Oxidative stress induces vascular calcification through modulation of the osteogenic transcription factor Runx2 by AKT signaling. *J Biol Chem* 283: 15319–15327, 2008.
10. Campisi J. Cancer and ageing: rival demons? *Nat Rev Cancer* 3: 339–349, 2003.
11. Cortassa S, O'Rourke B, and Aon MA. Redox-optimized ROS balance and the relationship between mitochondrial respiration and ROS. *Biochim Biophys Acta* 1837: 287–295, 2014.
12. Dai DF, Santana LF, Vermulst M, Tomazela DM, Emond MJ, MacCoss MJ, Gollahon K, Martin GM, Loeb LA, Ladiges WC, and Rabinovitch PS. Overexpression of catalase targeted to mitochondria attenuates murine cardiac aging. *Circulation* 119: 2789–2797, 2009.
13. Dalle-Donne I, Aldini G, Carini M, Colombo R, Rossi R, and Milzani A. Protein carbonylation, cellular dysfunction, and disease progression. *J Cell Mol Med* 10: 389–406, 2006.
14. Desai LP, Zhou Y, Estrada AV, Ding Q, Cheng G, Collawn JF, and Thannickal VJ. Negative regulation of NADPH oxidase 4 by hydrogen peroxide-inducible clone 5 (Hic-5) protein. *J Biol Chem* 289: 18270–18278, 2014.
15. Dikalova AE, Bikineyeva AT, Budzyn K, Nazarewicz RR, McCann L, Lewis W, Harrison DG, and Dikalov SI. Therapeutic targeting of mitochondrial superoxide in hypertension. *Circ Res* 107: 106–116, 2010.
16. d'Uscio LV, Baker TA, Mantilla CB, Smith L, Weiler D, Sieck GC, and Katusic ZS. Mechanism of endothelial dysfunction in apolipoprotein E-deficient mice. *Arterioscler Thromb Vasc Biol* 21: 1017–1022, 2001.
17. England K and Cotter TG. Direct oxidative modifications of signalling proteins in mammalian cells and their effects on apoptosis. *Redox Rep* 10: 237–245, 2005.
18. Go AS, Mozaffarian D, Roger VL, Benjamin EJ, Berry JD, Blaha MJ, Dai S, Ford ES, Fox CS, Franco S, Fullerton HJ, Gillespie C, Hailpern SM, Heit JA, Howard VJ, Huffman MD, Judd SE, Kissela BM, Kittner SJ, Lackland DT, Lichtman JH, Lisabeth LD, Mackey RH, Magid DJ, Marcus GM, Marelli A, Matchar DB, McGuire DK, Mohler ER, 3rd, Moy CS, Mussolino ME, Neumar RW, Nichol G, Pandey DK, Paynter NP, Reeves MJ, Sorlie PD, Stein J, Towfighi A, Turan TN, Virani SS, Wong ND, Woo D, Turner MB, and on behalf of the American Heart Association Statistics Committee and Stroke Statistics Subcommittee. Heart disease and stroke statistics—2014 update: a Report From the American Heart Association. *Circulation* 129: e28–e292, 2014.
19. Goldsteins G, Keksa-Goldsteine V, Ahtoniemi T, Jaronen M, Arens E, Akerman K, Chan PH, and Koistinaho J. Deleterious role of superoxide dismutase in the mitochondrial intermembrane space. *J Biol Chem* 283: 8446–8452, 2008.
20. Han Z, Chen YR, Jones CI, 3rd, Meenakshisundaram G, Zweier JL, and Alevriadou BR. Shear-induced reactive nitrogen species inhibit mitochondrial respiratory complex activities in cultured vascular endothelial cells. *Am J Physiol Cell Physiol* 292: C1103–C1112, 2007.
21. He C, Murthy S, McCormick ML, Spitz DR, Ryan AJ, and Carter AB. Mitochondrial Cu,Zn-superoxide dismutase mediates pulmonary fibrosis by augmenting H_2O_2 generation. *J Biol Chem* 286: 15597–15607, 2011.
22. Hecker L, Logsdon NJ, Kurundkar D, Kurundkar A, Bernard K, Hock T, Meldrum E, Sanders YY, and Thannickal VJ. Reversal of persistent fibrosis in aging by targeting Nox4-Nrf2 redox imbalance. *Sci Transl Med* 6: 231ra47, 2014.
23. Hulsmans M, Van Dooren E, and Holvoet P. Mitochondrial reactive oxygen species and risk of atherosclerosis. *Curr Atheroscler Rep* 14: 264–276, 2012.
24. Jiang JX, Chen X, Serizawa N, Szyndralewiez C, Page P, Schroder K, Brandes RP, Devaraj S, and Torok NJ. Liver fibrosis and hepatocyte apoptosis are attenuated by GKT137831, a novel NOX4/NOX1 inhibitor *in vivo*. *Free Radic Biol Med* 53: 289–296, 2012.
25. Judkins CP, Diep H, Broughton BR, Mast AE, Hooker EU, Miller AA, Selemidis S, Dusting GJ, Sobey CG, and Drummond GR. Direct evidence of a role for Nox2 in superoxide production, reduced nitric oxide bioavailability, and early atherosclerotic plaque formation in $ApoE^{-/-}$ mice. *Am J Physiol Heart Circ Physiol* 298: H24–H32, 2010.
26. Kuroda J, Ago T, Matsushima S, Zhai P, Schneider MD, and Sadoshima J. NADPH oxidase 4 (Nox4) is a major source of oxidative stress in the failing heart. *Proc Natl Acad Sci U S A* 107: 15565–15570, 2010.
27. Laleu B, Gaggini F, Orchard M, Fioraso-Cartier L, Cagnon L, Houngninou-Molango S, Gradia A, Duboux G, Merlot C, Heitz F, Szyndralewiez C, and Page P. First in class, potent, and orally bioavailable NADPH oxidase isoform 4 (Nox4) inhibitors for the treatment of idiopathic pulmonary fibrosis. *J Med Chem* 53: 7715–7730, 2010.
28. Lassegue B, San Martin A, and Griendling KK. Biochemistry, physiology, and pathophysiology of NADPH oxidases in the cardiovascular system. *Circ Res* 110: 1364–1390, 2012.
29. Liberman M, Bassi E, Martinatti MK, Lario FC, Wosniak J, Jr., Pomerantzeff PM, and Laurindo FR. Oxidant generation predominates around calcifying foci and enhances progression of aortic valve calcification. *Arterioscler Thromb Vasc Biol* 28: 463–470, 2008.
30. Luo C, Long J, and Liu J. An improved spectrophotometric method for a more specific and accurate assay of mitochondrial complex III activity. *Clin Chim Acta* 395: 38–41, 2008.
31. Madamanchi NR and Runge MS. Mitochondrial dysfunction in atherosclerosis. *Circ Res* 100: 460–473, 2007.
32. Madamanchi NR and Runge MS. Redox signaling in cardiovascular health and disease. *Free Radic Biol Med* 61C: 473–501, 2013.
33. Madamanchi NR, Vendrov A, and Runge MS. Oxidative stress and vascular disease. *Arterioscler Thromb Vasc Biol* 25: 29–38, 2005.
34. Mattace-Raso FU, van der Cammen TJ, Hofman A, van Popele NM, Bos ML, Schalekamp MA, Asmar R, Reneman RS, Hoeks AP, Breteler MM, and Witteman JC. Arterial stiffness and risk of coronary heart disease and stroke: the Rotterdam Study. *Circulation* 113: 657–663, 2006.
35. Mercer JR, Cheng KK, Figg N, Gorenne I, Mahmoudi M, Griffin J, Vidal-Puig A, Logan A, Murphy MP, and Bennett M. DNA damage links mitochondrial dysfunction to atherosclerosis and the metabolic syndrome. *Circ Res* 107: 1021–1031, 2010.
36. Mookerjee SA, Divakaruni AS, Jastroch M, and Brand MD. Mitochondrial uncoupling and lifespan. *Mech Ageing Dev* 131: 463–472, 2010.

37. Moon SK, Thompson LJ, Madamanchi N, Ballinger S, Papaconstantinou J, Horaist C, Runge MS, and Patterson C. Aging, oxidative responses, and proliferative capacity in cultured mouse aortic smooth muscle cells. *Am J Physiol Heart Circ Physiol* 280: H2779–H2788, 2001.
38. Moukdar F, Robidoux J, Lyght O, Pi J, Daniel KW, and Collins S. Reduced antioxidant capacity and diet-induced atherosclerosis in uncoupling protein-2-deficient mice. *J Lipid Res* 50: 59–70, 2009.
39. National Cholesterol Education Program (NCEP) Expert Panel on Detection, Evaluation, and Treatment of High Blood Cholesterol in Adults (Adult Treatment Panel III). Third Report of the National Cholesterol Education Program (NCEP) expert panel on detection, evaluation, and treatment of high blood cholesterol in adults (adult treatment panel III) final report. *Circulation* 106: 3143–3421, 2002.
40. Ng K, Hildreth CM, Phillips JK, and Avolio AP. Aortic stiffness is associated with vascular calcification and remodeling in a chronic kidney disease rat model. *Am J Physiol Renal Physiol* 300: F1431–F1436, 2011.
41. Nisimoto Y, Diebold BA, Cosentino-Gomes D, and Lambeth JD. Nox4: a hydrogen peroxide-generating oxygen sensor. *Biochemistry* 53: 5111–5120, 2014.
42. Porteous CM, Logan A, Evans C, Ledgerwood EC, Menon DK, Aigbirhio F, Smith RA, and Murphy MP. Rapid uptake of lipophilic triphenylphosphonium cations by mitochondria *in vivo* following intravenous injection: implications for mitochondria-specific therapies and probes. *Biochim Biophys Acta* 1800: 1009–1017, 2010.
43. Ray R, Murdoch CE, Wang M, Santos CX, Zhang M, Alom-Ruiz S, Anilkumar N, Ouattara A, Cave AC, Walker SJ, Grieve DJ, Charles RL, Eaton P, Brewer AC, and Shah AM. Endothelial Nox4 NADPH oxidase enhances vasodilatation and reduces blood pressure *in vivo*. *Arterioscler Thromb Vasc Biol* 31: 1368–1376, 2011.
44. Rodriguez-Manas L, El-Assar M, Vallejo S, Lopez-Doriga P, Solis J, Petidier R, Montes M, Nevado J, Castro M, Gomez-Guerrero C, Peiro C, and Sanchez-Ferrer CF. Endothelial dysfunction in aged humans is related with oxidative stress and vascular inflammation. *Aging Cell* 8: 226–238, 2009.
45. Sanders YY, Liu H, Liu G, and Thannickal VJ. Epigenetic mechanisms regulate NADPH oxidase-4 expression in cellular senescence. *Free Radic Biol Med* 79: 197–205, 2015.
46. Sedeek M, Callera G, Montezano A, Gutsol A, Heitz F, Szyndralewiez C, Page P, Kennedy CR, Burns KD, Touyz RM, and Hebert RL. Critical role of Nox4-based NADPH oxidase in glucose-induced oxidative stress in the kidney: implications in type 2 diabetic nephropathy. *Am J Physiol Renal Physiol* 299: F1348–F1358, 2010.
47. Serrander L, Cartier L, Bedard K, Banfi B, Lardy B, Plastre O, Sienkiewicz A, Forro L, Schlegel W, and Krause KH. NOX4 activity is determined by mRNA levels and reveals a unique pattern of ROS generation. *Biochem J* 406: 105–114, 2007.
48. Sheehan AL, Carrell S, Johnson B, Stanic B, Banfi B, and Miller FJ, Jr. Role for Nox1 NADPH oxidase in atherosclerosis. *Atherosclerosis* 216: 321–326, 2011.
49. Sorescu D, Weiss D, Lassegue B, Clempus RE, Szocs K, Sorescu GP, Valppu L, Quinn, MT, Lambeth JD, Vega JD, Taylor WR, and Griendling KK. Superoxide production and expression of nox family proteins in human atherosclerosis. *Circulation* 105: 1429–1435, 2002.
50. Stary HC, Chandler AB, Glagov S, Guyton JR, Insull W, Rosenfeld ME, Schaffer SA, Schwartz CJ, Wagner WD, and Wissler RW. A definition of initial, fatty streak, and intermediate lesions of atherosclerosis. A report from the Committee on vascular lesions of the council on arteriosclerosis, american heart association. *Circulation* 89: 2462–2478, 1994.
51. Steed MM, Tyagi N, Sen U, Schuschke DA, Joshua IG, and Tyagi SC. Functional consequences of the collagen/elastin switch in vascular remodeling in hyperhomocysteinemic wild-type, $eNOS^{-/-}$, and $iNOS^{-/-}$ mice. *Am J Physiol Lung Cell Mol Physiol* 299: L301–L311, 2010.
52. Stocker R and Keaney JF, Jr. Role of oxidative modifications in atherosclerosis. *Physiol Rev* 84: 1381–1478, 2004.
53. Takabe W, Li R, Ai L, Yu F, Berliner JA, and Hsiai TK. Oxidized low-density lipoprotein-activated c-Jun NH2-terminal kinase regulates manganese superoxide dismutase ubiquitination: implication for mitochondrial redox status and apoptosis. *Arterioscler Thromb Vasc Biol* 30: 436–441, 2010.
54. Takac I, Schroder K, Zhang L, Lardy B, Anilkumar N, Lambeth JD, Shah AM, Morel F, and Brandes RP. The E-loop is involved in hydrogen peroxide formation by the NADPH oxidase Nox4. *J Biol Chem* 286: 13304–13313, 2011.
55. Tchivilev I, Madamanchi NR, Vendrov AE, Niu XL, and Runge MS. Identification of a protective role for protein phosphatase 1cgamma1 against oxidative stress-induced vascular smooth muscle cell apoptosis. *J Biol Chem* 283: 22193–22205, 2008.
56. Thannickal VJ, Zhou Y, Gaggar A, and Duncan SR. Fibrosis: ultimate and proximate causes. *J Clin Invest* 124: 4673–4677, 2014.
57. Ungvari Z, Kaley G, de Cabo R, Sonntag WE, and Csiszar A. Mechanisms of vascular aging: new perspectives. *J Gerontol A Biol Sci Med Sci* 65: 1028–1041, 2010.
58. Ungvari Z, Orosz Z, Labinskyy N, Rivera A, Xiangmin Z, Smith K, and Csiszar A. Increased mitochondrial H2O2 production promotes endothelial NF-kappaB activation in aged rat arteries. *Am J Physiol Heart Circ Physiol* 293: H37–H47, 2007.
59. van Popele NM, Grobbee DE, Bots ML, Asmar R, Topouchian J, Reneman RS, Hoeks AP, van der Kuip DA, Hofman A, and Witteman JC. Association between arterial stiffness and atherosclerosis: the Rotterdam Study. *Stroke* 32: 454–460, 2001.
60. Vasa-Nicotera M, Chen H, Tucci P, Yang AL, Saintigny G, Menghini R, Mahe C, Agostini M, Knight RA, Melino G, and Federici M. miR-146a is modulated in human endothelial cell with aging. *Atherosclerosis* 217: 326–330, 2011.
61. Vendrov AE, Hakim ZS, Madamanchi NR, Rojas M, Madamanchi C, and Runge MS. Atherosclerosis is attenuated by limiting superoxide generation in both macrophages and vessel wall cells. *Arterioscler Thromb Vasc Biol* 27: 2714–2721, 2007.
62. Vendrov AE, Madamanchi NR, Hakim ZS, Rojas M, and Runge MS. Thrombin and NAD(P)H oxidase-mediated regulation of CD44 and BMP4-Id pathway in VSMC, restenosis, and atherosclerosis. *Circ Res* 98: 1254–1263, 2006.
63. Vendrov AE, Madamanchi NR, Niu XL, Molnar KC, Runge M, Szyndralewiez C, Page P, and Runge MS.

NADPH oxidases regulate CD44 and hyaluronic acid expression in thrombin-treated vascular smooth muscle cells and in atherosclerosis. *J Biol Chem* 285: 26545–26557, 2010.
64. Zhang L, Sheppard OR, Shah AM, and Brewer AC. Positive regulation of the NADPH oxidase NOX4 promoter in vascular smooth muscle cells by E2F. *Free Radic Biol Med* 45: 679–685, 2008.
65. Zhang M, Brewer AC, Schroder K, Santos CX, Grieve DJ, Wang M, Anilkumar N, Yu B, Dong X, Walker SJ, Brandes RP, and Shah AM. NADPH oxidase-4 mediates protection against chronic load-induced stress in mouse hearts by enhancing angiogenesis. *Proc Natl Acad Sci U S A* 107: 18121–18126, 2010.
66. Zhou RH, Vendrov AE, Tchivilev I, Niu XL, Molnar KC, Rojas M, Carter JD, Tong H, Stouffer GA, Madamanchi NR, and Runge MS. Mitochondrial oxidative stress in aortic stiffening with age: the role of smooth muscle cell function. *Arterioscler Thromb Vasc Biol* 32: 745–755, 2012.
67. Zielonka J, Hardy M, and Kalyanaraman B. HPLC study of oxidation products of hydroethidine in chemical and biological systems: ramifications in superoxide measurements. *Free Radic Biol Med* 46: 329–338, 2009.

Address correspondence to:
Prof. Marschall S. Runge
Department of Medicine
4107 Medical Sciences Building I
University of Michigan
Ann Arbor, MI 48109-5624

E-mail: mrunge@med.umich.edu

Date of first submission to ARS Central, December 10, 2014; date of final revised submission, May 19, 2015; date of acceptance, June 6, 2015.

Abbreviations Used

8-OHdG = 8-hydroxy-2′-deoxyguanosine
AK120765 = 2-(2-chlorophenyl)-4-methyl-5-(pyridin-2-ylmethyl)-1H-pyrazolo[4,3-c] pyridine-3,6(2H,5H)-dione
ALT = alanine aminotransferase
ANOVA = analysis of variance
BUN = blood urea nitrogen
CCCP = carbonyl cyanide *m*-chlorophenylhydrazone
CK = creatine kinase
CVD = cardiovascular disease
DAPI = 4′,6-diamidino-2-phenylindole
DHE = dihydroethidium
DMEM = Dulbecco's modified Eagle's medium
DPI = diphenyliodonium
ECG = electrocardiography
EIA = enzyme immunoassay
ETC = electron transport chain
FBS = fetal bovine serum
FCCP = Trifluoromethoxy carbonylcyanide phenylhydrazone
H&E = hematoxylin and eosin
HASMC = human aortic smooth muscle cell
HBSS = Hank's Balanced Salt Solution
HPLC = high-performance liquid chromatography
LV mass = left ventricle mass
LVEDV = left ventricle end-diastolic volume
LVEF = left ventricle ejection fraction
LVPWT = left ventricle posterior wall thickness
MitoTEMPO = (2-(2,2,6,6-tetramethylpiperidin-1-oxyl-4-ylamino)-2-oxoethyl) triphenylphosphonium chloride
mo = month-old
MOI = multiplicity of infection
mtROS = mitochondrial ROS
ND = normal chow diet
NDGA = nordihydroguaiaretic acid
NOX = NADPH oxidase
NS = not significant
OCR = oxygen consumption rate
PBS = phosphate-buffered saline
PEG = polyethylene glycol
PWV = pulse wave velocity
ROS = reactive oxygen species
SEM = standard error of the mean
SMA = smooth muscle actin
SOD2 = superoxide dismutase 2
TPP = triphenylphosphonium
VCAM = vascular cell adhesion molecule
VSMC = vascular smooth muscle cell
VSR = Verhoeff picrosirius red
WCL = whole cell lysate
WD = Western diet